Journal of Fluids and Structures 125 (2024) 104057

Contents lists available at ScienceDirect

Journal of Fluids and Structures

journal homepage: www.elsevier.com/locate/jfs

An experimental investigation into the effect two-phase flow induced vibrations have on a J-shaped flexible pipe

D.J. Pickles [a,*], G. Hunt [a], A.J. Elliott [b], A. Cammarano [a], G. Falcone [a]

[a] University of Glasgow, James Watt School of Engineering, UK
[b] Cranfield University, School of Aerospace, Transport and Manufacturing, UK

ARTICLE INFO

Keywords:
Fluid-structure interaction
Slug flow, Experiment
Multiphase flow
Flow Induced vibration

ABSTRACT

Multiphase flow inside of pipes occurs in a wide variety of engineering applications, including offshore deep-water oil and gas transport. Vibrations induced by the flow inside of the pipe can lead to its mechanical failure and thus lead to uncontrolled release of the fluids being transported. In subsea applications, flexible J-risers are often employed to deliver the produced fluids from the seafloor to the host platform. Despite the potentially significant liabilities associated with subsea hydrocarbon leaks, there has been a distinct lack of investigations into how flow induced vibrations in large scale, pressurised flexible J-risers can lead to system integrity loss. Previous investigations have generally focused on the response of rigid pipes or small scale, unpressurised flexible risers. This study presents an investigation into the response of a 10 m long, 50.8 mm internal diameter composite riser containing a tensile armour helical structure to a variety of two-phase, water-nitrogen flows at 10.8 barg of pressure and ambient temperature. High speed cameras were used to investigate the structure of the flow at either end of the flexible riser, whilst synchronised surface mounted strain gauges and accelerometers were used to investigate the response of the pipe. Time-averaged data were acquired to assess the general response of the pipe, whilst a statistical analysis of the fluctuations highlighted the movement of the pipe. One-dimensional and computational fluid dynamics simulations were used to define the experimental test matrix and provide further insight into the structure of the flow inside the J-riser. Single-phase gas flow was found not to cause the J-riser to move significantly, whilst multiphase flow led to significant in-plane movement of the pipe. Increasing the liquid flow rate (or decreasing the gas flow rate) increased the mean strain experienced by the pipe. At low gas flow rates, the pipe oscillated smoothly about its mean position, but at higher gas flow rates a violent intermittent whipping motion was observed. The latter produced large in-plane and out-of-plane movement of the pipe which could pose a threat to system integrity. This work offers new insights into fluid-structure interactions in large scale engineering applications, contributing to improved system design and control.

1. Introduction

Two-phase, gas-liquid flows are frequently observed in a variety of industrial processes, including sewage systems, power and processing plants, and pipelines conveying oil and gas prior to separation. Depending on the operating conditions of the system,

* Corresponding author.
E-mail address: djpickles2@gmail.com (D.J. Pickles).

https://doi.org/10.1016/j.jfluidstructs.2023.104057
Received 22 May 2023; Received in revised form 21 December 2023; Accepted 24 December 2023

different flow regimes may occur, some of which can lead to vibrations or mechanical failure (Wang et al., 2018a). Pipes conveying multiphase flow can result in several possible flow regimes. In two-phase gas-liquid flow, for a given total volumetric flux, the highest maximum force fluctuations were found in the slug or churn flow regimes (Liu et al., 2012). Gas-liquid flow at relatively low velocities results in a stratified flow regime in a horizontal pipe, where the gas flows over the top of the liquid, without disturbance. At increased velocities the surface of the liquid becomes agitated resulting in waved stratified flow. Further increases in velocity causes these waves to increase in height until they reach the top of the pipe, at which point slug flow has developed (Dukler and Hubbard, 1971). Each slug unit consists of a liquid slug and a slug bubble (sometimes referred to as a Taylor bubble) alternately. That is not to say that inlet conditions which consist of stratified or waved stratified flow can not produce significant vibrations as clearly from the above discussion, both stratified and waved stratified flow at the inlet can lead to slug flow under the correct conditions. Studies on the vibrations produced by stratified and waved stratified flow have been conducted both numerically and experimentally (Miwa et al., 2016). Taking into account the collisional effects resulting from gas-liquid waves with the structure of the bend, the researchers recognised that collision forces and momentum fluctuations associated with the waves were important when considering the vibrations it may cause. Additionally, the transient cyclic event known as severe slugging may occur in pipeline-riser systems at relatively low flow rates and stratified inlet conditions and can cause significant fluctuations in both pressure and flow rate (Malekzadeh et al., 2012.). In addition to experimental and computational fluid dynamic (CFD) studies, several other novel techniques have been brought to bear on the problems associated with slug flow in pipes. One example of such a technique was used by researchers who contended that for high aspect ratio pipes, the computational load to apply a CFD approach is prohibitive (Heaney et al., 2022). To combat this, the use of AI assisted modelling was employed in the form of non-intrusive reduced-order modelling (NIROM) as a potential tool to alleviate the issues of high computing time and computational power. The researchers succeeded in making predictions based on a 10 m pipe for training to gain results for a 98 m pipe resulting in realistic predictions for this extended pipe. Another novel approach to investigating slug flow was to apply a one-dimensional mechanistic model to predict gas–liquid slug flow in a riser like configuration using slug tracking (Padrino et al., 2023).

Fluid-structure interaction (FSI) is a field of study concerned with the coupling between a rigid or deformable material and a fluid flow. This may be either internal flow-induced vibration (FIV) or external to the structure such as vortex induced vibration (VIV). Studies on the effect of VIV on flexible pipes, which are of interest to this study, have been performed experimentally to understand how spacing between such risers affect vibrational response (Xu et al., 2020). The wake patterns produced by the flow past one such riser may induce vibrations in the next riser along. This phenomenon was investigated using direct numerical simulation (DNS) arranging the cylinders in a triangular formation rather than a side-by-side formation (Chen et al., 2022). The researchers noted that both an in-phase and out of phase wake pattern hysteresis effect was produced when increasing or decreasing reduced velocity (reduced velocity relates the bulk velocity to the natural frequency and cylinder diameter) respectively. The vibration response of such a small inner diameter riser to an external log-law shear flow was examined for how the modes of the pipe responded both in space and time (Zhu et al., 2021b). While VIV is an important contributor to structural fatigue in subsea to surface oil and gas risers, the focus of this study in on internal flow-induced vibration. Early work in this area focused on horizontal pipes in the first instance. It was proposed that the variation in density associated with alternate gas and liquid slugs are the source of the momentum flux and this induced the vibration (Yih and Griffith, 1968). Confirmation of the contribution to pipe vibration due to density differences was delivered soon thereafter (Hara, 1973). Applying a combined experimental and theoretical approach, it was demonstrated that the greatest vibrational response was induced when the ratio of the pipe natural frequency to the slug frequency was 0.5, 1.0 and 1.5 (Hara and Yamashita, 1978). Similar findings have been observed by other researchers, whereby when the slug frequency coincides with the natural frequency of the structure, the interaction between the flow and structure FIV is greatly amplified. In nuclear power plants, the main steam lines can be subject to pressure pulses, which may induce resonance if the pulse frequency is close to that of the structure (Pettigrew et al., 1998). Using a combination of experiments and numerically modelling of hydrodynamic slug flow in horizontal pipes it was found that the flow velocity of the slugs has a strong effect on the vibrational response (Wang et al., 2018a). A clamped-clamped horizontal poly vinyl chloride (PVC) pipe with 20.4 mm I.D. subject to air-water multiphase flow was examined to investigate the dynamic response (Ortiz-Vidal et al., 2017). It was demonstrated that the induced vibrations on the structure were sensitive to the gas-liquid flow velocity, void fraction, and flow regime. A comprehensive review of factors affecting internal two-phase flow induced vibrations was performed by Khan et al. (Khan et al., 2022). A brief summary of important parameters that affect the FIV caused by multiphase flows is described in the following.

The geometry of rigid pipes, specifically pipe diameter and bends (e.g., 90° bends, T-junctions) may significantly influence the flow-induced vibrations caused by internal two-phase flows. Considering first the effect of pipe diameter upon FIV. Increasing the diameter of the pipe increases the excitation forces whilst decreasing the dominant frequency. However, the response of large diameter pipes differs considerably from that of smaller diameter pipes (Schlegel et al., 2012). While working with vertical cylindrical two-phase flow, where gravity head is important, pipes were characterised by Schlegel et al. as large or small based on the non-dimensional hydraulic diameter, D_H^*:

$$D_H^* = \frac{D_H}{\sqrt{\sigma/g\Delta\rho}} \tag{1}$$

Where D_H, g, σ and $\Delta\rho$ are the hydraulic diameter, gravitational acceleration, liquid phase surface tension and the density difference between the two phases respectively. Small pipes have $D_H^* < 18.6$ and larger pipes have $D_H^* > 40$. For $18.6 < D_H^* < 40$, the pipe is defined as being in the transition region and therefore experiences flow features associated with both small and large pipes, such as the bubbly flow regime. In smaller diameter pipes, with increasing superficial velocities the flow transitions to a stable slug flow regime.

Whereas, in larger diameter pipes, the flow enters the bubbly flow regime, and then a churn turbulent flow regime (Schlegel et al., 2012). This is due to the inability of larger diameter pipes to tolerate slug bubbles that fill the whole cross-section of the pipe because of the Raliegh-Taylor instability (Schlegel et al., 2012). The forces experienced by larger diameter pipes are significantly larger than those of smaller diameter pipes, according to a validated numerical modelling approach (Chinenye-Kanu et al., 2019). Secondly, considering the effects associated with different types of bend. FIV can also occur in conduits featuring curvature whereby the slug units may collide with the structure's surface as they pass, thereby transmitting the intermittent forces created by the momentum and pressure differential. Conditions like these are experienced in a variety of engineering applications, such as oil pipelines, chemical systems, and the nuclear industry (Abdulkadir et al., 2019; Gourma and Verdin, 2020; Mohmmed et al., 2020). The amplitude and frequency of the force fluctuations, experienced by 90° bends and U-bends in response to slug/churn flow increased with flow velocity for the volumetric flow rates investigated (Liu et al., 2012; Riverin et al., 2006; Riverin and Pettigrew, 2007). Investigation of a 90° bend in a horizontal stainless-steel pipe with 70 mm inner diameter (ID) and a bend radius of 105 mm was conducted to determine the effect of liquid viscosity and surface tension on the maximum forces acting on the bend (Tay and Thorpe, 2004). The researchers used isopropanol and glycerol solutions to vary the liquid viscosity by −32 % and surface tension by +162 % with respect to the properties of an air-water flow. No significant change on the magnitude of the maximum forces was observed with either of the changes to the liquid properties. Examination of vertical U-bends featuring two 90° bends 300 mm apart in a 20.6 mm ID PVC tube were conducted to determine a common formulation of the forces at work, in such bends, by characterising the rms (root mean square) of the excitation forces (Riverin et al., 2006). The researchers were able to correlate the rms of the force to the Weber number for a range of bends and T-junctions and numerous flow conditions. In a later work, experiments using an increased range of bend radii from dimensionless bend radius, R/d, of 0.5 to 7.2 were performed (Riverin and Pettigrew, 2007). It was observed that when the frequency of the excitation forces of the flow and the frequency of the structure coincided resonance effects produced significant in-plane vibrational responses. Additionally, as mentioned previously, it was found that flow velocity increase was associated with an increase in the rms of the force fluctuation. An experimental investigation of the fluctuating force caused by two-phase flow on a 52.5 mm ID, 76.2 mm radius, 90° elbow in a vertical orientation demonstrated that the maximum force fluctuations occurred as the flow regime traversed from bubbly to slug flow (Liu et al., 2012). Also, increasing the gas superficial velocity, whilst maintaining a constant liquid superficial velocity increased the fluctuating forces experienced by the pipe monotonically. A horizontal 1″ pipe system under two-phase air-water slug flow conditions, was used to examine multiple bend structures responses to a range of flow regimes (Belfroid et al., 2011). This revealed a maximum of 4 orders of magnitude higher response for slug flow than in single phase flow for comparable velocities. Each of these studies confirmed that the effect was down to the flow regime rather that the specific value of the void fraction, indicating that it is imperative that the two-phase flow regime is correctly identified for any such analysis of FIV (Miwa et al., 2015). Changes in flow regime significantly affects the forces experienced by pipes, further highlighting the importance of the correct characterisation of the flow regime within the pipe (Miwa et al., 2015). For horizontal-horizontal U-bend structures it has been found that the greatest peak hydrodynamic forces were found in the pseudo-slug flow regime (the transition between slug flow and annular flow) in experimental tests (Garcia et al., 2023). However, the researchers posited that considering only the magnitude of the force did not determine the greatest chance of structural fatigue and that the higher frequencies associated with slug flow could be more harmful. Combining both the effects associated with bends and with pipe diameter, numerical modelling of FIV forces at 90° elbows was carried out to examine the effect of pipe diameter (Asiegbu et al., 2023). The modelling results showed that the behaviours of the FIV at the pipe elbow as a function of gas velocity for both small and large internal diameters are similar. However, the force characteristics in the intermediate diameter pipe behaved differently. The authors attributed this to the transition behaviour of the flow induced by Taylor instability in this intermediate sized pipe.

Studies on rigid pipes have been dominated by pipes in either horizontal or vertical orientations. Straight pipes were tested at 0°, 30°, 45°, 60° and 90° inclination to the horizontal for the purpose of investigating the effect of gravity on the two-phase flow behaviour (Jagan and Satheesh, 2016). The authors discovered that stratified flow and stratified waved flow was only observed in the horizontal pipe and does not appear in any of the inclinations tested. Thus, for pipes which deviate from the horizontal, the flow regime map within the pipe must be reconsidered taking this information into account. Flow regime maps for inclined pipes have been made for a number of both upward and downward inclinations from 0 to 10° (Barnea et al., 1980). In agreement with previous researchers, smooth stratified flow was not observed except at very low inclinations. Researchers found that inclination's effect on flow patterns was greatest at the transition between stratified and intermittent/annular regimes. It should be noted that these studies involved pipes featuring constant gradient and not varying gradients associated with curved pipes.

The discussed studies have thus far concentrated on pipe systems featuring high levels of rigidity. Consideration to the responses of flexible pipes to internal slug flow are less frequent. Experiments to study the fluidelastic structural response of cantilevered flexible tubes to internal two-phase air–water internal flow were conducted (Monette and Pettigrew, 2004). Using flexible tubes of different diameters, lengths and flexural rigidities tests were performed by the researchers over a wide range of flow velocities and void fractions. Interestingly, it was observed that for a given pipe that undergoes instability in the first mode in air and in the fourth mode in water, the instabilities in the first to fourth mode are also observed in two-phase flows. However, these instability modes are not stationary, in fact, the nodes were seen to move along the tube. This node migration is attributed to the results of an infinite addition of normal modes, which the researchers described by the fluidelastic instability response equation that was presented.

In real world industrial applications, many pipes are influenced by the terrain (Gourma and Verdin, 2016; Yang et al., 2018) or design necessity, such as J-risers from subsea to floating rig (Wang et al., 2018b). Studies of curved pipes are less common than those featuring rigid geometry (Padrino et al., 2023). Subsea to surface flexible risers in oil and gas facilities are known to have a complex series of structural component layers (Zhang et al., 2023). An important component of such j-risers are tensile armours, these are the

primary load-bearing structures of the riser. They have a helical shape, which is wound layer by layer during the manufacturing process in a specific spiral. Typically, they have a rectangular cross section with a constant pitch angle at every layer. The specific spiral pitch angles are designed to accommodate the required tensile load (Zhang et al., 2023). For large diameter, long axial length flexible pipes, like those used for offshore risers it was indicated that fluid weight, curvature induced load, centrifugal and Coriolis effects of the flow momentum would affect the response of the pipe when compared to these smaller scale investigations (Patel and Seyed, 1989). The modelling they performed indicated that slug induced vibrations can modify the riser's geometric stiffness and the pipe's dynamic tension. In contrast to vertical pipes, it was discovered that the pressure at the base of a catenary riser increased more slowly due to its curved geometry (Duan et al., 2017). Investigations using a gas-liquid flow rate ratio range of 0.5–1.827 on small diameter (6 mm ID), small scale pipes, revealed that slug flow inside the pipes can cause it to move in-plane (Zhu et al., 2018). The researchers also found that the second-order mode provided the dominant response in the pipe structure. Further, it was shown that slug flow features, such as slug length, ratio of gas to liquid phase, and superficial velocity, influenced the amplitude of the observed vibrations. When the gas-liquid ratio is increased to 3.031, the in-plane response is dominated by the first mode of motion of the pipe (Zhu et al., 2019). The highest vibrational responses were observed to coincide with the longest length slugs. Travelling waves, associated with the passage of large liquid slugs passing through the flexible riser generated larger amplitude pipe movements (Zhu et al., 2019). An investigation of severe slug flow in a high aspect ratio flexible catenary riser experiment using a 1.2 m length, 6 mm ID pipe was carried out by researchers. The dynamic response of the riser was observed to be linked to the liquid slug length, and liquid inventory along the J-riser, generating a resonance between the oscillation measured and the fluid pressure fluctuation (Zhu et al., 2021a). Additionally, an unstable oscillation containing alternate long slugs and short slugs was observed. These flow patterns deviate from the reported flow regimes in large-scale pipes, the researchers attribute this to the effect of surface tension in such a small diameter riser system (Zhu et al., 2021a).

Studies related to the response of flexible curved pipes to internal slug flow are infrequent (Zhu et al., 2018), so the understanding of slug flow induced vibrations in flexible J-riser shaped pipes is limited. The above review of the literature highlights a number of issues yet to be addressed. Flow regime maps for rigid straight pipes are well documented. For horizontal-vertical curved pipes, as opposed to pipes curving in the horizontal plane, the question of how these flow regime maps compare to the flow regimes that manifest there is not understood. The extent to which a rigid geometry numerical model can correctly predict the flow regime type for a flexible structure is investigated in this study. The bulk of the findings on flexible riser systems are based on small diameter pipes and flow behaviour in small pipes differs to that of larger pipes (Schlegel et al., 2012). Conclusions drawn from the behaviour of small pipes might not be applicable to larger pipes (Khan et al., 2022). Given that surface tension may cause deviation from flow patterns in small scale pipes (Zhu et al., 2021a), it is not known if intermediate scale pipes conform to the flow patterns. All prior studies have used a single material composition for the pipes investigated, be it steel or PVC. The studies on the flexible risers pioneered by Zhu et al. (Zhu et al., 2021a, 2019, 2018) have focused on single material risers. The questions as to how a composite riser structure containing a tensile armour helical structure responded to internal FIV stimulation have not been addressed in previous experimental studies.

In this study, the response of a intermediate diameter, pressurised, long length, tensile armoured flexible J-riser to a variety of two phase, water/nitrogen flow conditions are investigated experimentally. Surface mounted accelerometers and strain gauges were used to investigate the response of the J-riser, whilst custom PVC viewing sections installed at either end of the flexible riser allowed the visualisation and characterisation of the flow entering and exiting the flexible pipe. It was theorised that the J-riser would influence the flow regime entering the riser, therefore multiple techniques were employed in advance of the experiments on a rigid J-riser to ensure that the flow entering the J-riser was correctly characterised.

2. Experimental design

2.1. Test matrix design

To ensure that the relationship between slug flow characteristics and structural response is properly determined, a comprehensive matrix of test points in and close to the slug flow regime was sought. As mentioned in Section 1, while the void fraction is of interest, it is paramount that the correct flow regime is identified. To ensure that slug flow characteristics were obtained, a comprehensive matrix of test points in and close to the slug regime was investigated. Limiting factors placed on the choice of test points, in addition to the slug flow requirement, were that the gas flow rate had to be greater than 5 m^3/hr. The reason being that this was the lower limit to which gas flow was calibrated in the TÜV SÜD National Engineering Laboratory's Advanced Multiphase Facility (AMF). Total velocity, u_t, and a range of flow rates of 2–5 ms^{-1} were specified so that the flow did not pass through the 10 m riser at dangerously high velocities. The superficial velocity of a phase is the velocity at which that phase would travel through the pipe were it the only phase present. This value is calculated by dividing the liquid and gas flow rates by the cross-sectional area of the pipe (Widyatama et al., 2016). Where the fluid densities were determined at 10 barg pressure and 20 °C temperature conditions. The total velocity is equal to the sum of the superficial velocities of the liquid, u_l, and gas, u_g, phases such that:

$$U_t = U_{sl} + U_{sg} \tag{2}$$

Based on these stipulations, a suitable window for gas and liquid flow rate were ascertained through the spreadsheet digitized from Shell DEP 31.22.05.11 ("Flow regime map for two-phase flow 2011), which are defined in terms of the respective superficial velocities. Since the flow regime entering the riser was the primary focus of the modelling, the horizontal flow regime map was prioritized. To this end, a test matrix was generated, initially using a broad range of test points from the Shell flow regime map. As described in Section 1,

there are a wide range of possible superficial velocity combinations that combine to give slug flow on the flow regime map. These were then examined via the one-dimensional multiphase flow software package, PETEX GAP, and those that were predicted to generate slug flow were further examined using commercial CFD package Star-CCM+ (version 15.04.010) to aid the choice of the final test matrix. Points that had been predicted by the horizontal flow regime map to fall within the slug flow regime, but failed to produce the required flow regime during this process were discarded. Those that remained were then simulated using CFD where, similarly, the test points which failed to yield slug flow at the inlet were discarded. This was the sole purpose of the CFD, to aid and de-risk the preparation for the large scale experimental campaign. To reduce the number of potential test points from the flow map, PETEX GAP was used in the first instance.

2.1.1. PETEX gap model

To explore suitable test points further, the one-dimensional multiphase flow software package, PETEX GAP was used to assess the flow regime as it progressed along the pipeline. The riser was modelled by discretizing a quarter ellipse with major and minor axes of length 7.7 *m* and 5 *m*, respectively. Since the exact shape that the riser would take once connected to the rig was not known prior to the set-up of the experiments, some assumptions had to be made. It was known that the connection to the bottom of the riser would be horizontal and at the top, vertical. Additionally, the riser was known to have a 5 *m* vertical drop based on the available structure at the test facility. Due to the flexibility of the pipe, the shape taken by the pipe under pressure and when containing a varying mass of liquid could not be tested before the experiment was set up. Plotting the catenary curve for a *10 m* riser length with a drop of *5 m* revealed that while the riser is horizontal at the origin, it approaches the vertical viewing section's position (see Fig. 1) at a significant deviation from vertical. In fact, using the catenary equation the gradient at the intersection with the vertical viewing section's position is calculated to be 1.33. This gives an angle of 52° with the horizontal. This is a significant deviation from the vertical attachment condition required. Forcing the attachment to be vertical will clearly cause the path of the pipe to deviate significantly from the catenary curve. Taking this into account, it was decided that a quarter ellipse profile would provide a good approximation, and this determined the horizontal length of 7.7 *m* based on the 10 *m* total length of the pipe. A straight, horizonal region was added to permit flow development prior to entering the riser section with a short horizontal viewing section (see Fig. 1).

For the GAP simulations, the system was assumed to be rigid, so that suitable test points could be identified solely based on their predicted flow regime behavior without pipe displacement. While the GAP simulations largely confirmed the findings from the Shell DEP 31.22.05.11 flow regime map, some additional insight was provided. First, several of the test points that were predicted to exhibit

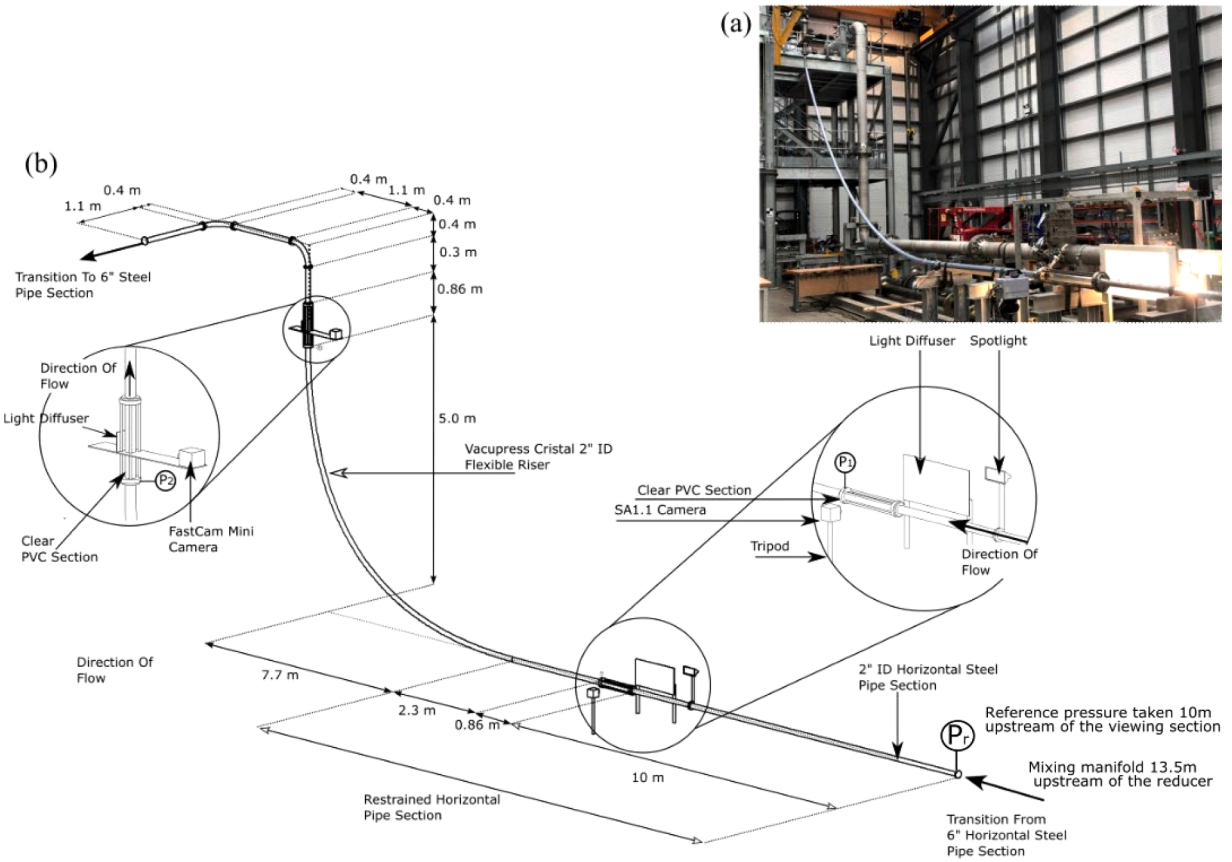

Fig. 1. Experimental set up depicted as a) photographic representation (inset) and b) schematic representation detailing associated lengths.

slug flow by the Shell flow regime map were determined to be in the 'stratified wavy' regime by GAP. These test points highlighted the challenges in predicting flow character close to the flow regime boundary. These uncertainties were accommodated for by filtering the potential test point through PETEX GAP initially, then through CFD secondly, and only those test points that exhibited slug flow in both GAP and CFD were passed to the experimental stage. Those that did not meet the criterion of slug flow at the entrance to the riser were discarded. Many test points remained valid at this stage, so further filtering of test points was required. This was accomplished using CFD.

2.1.2. Computational model

Increased confidence in the achievement of slug flow entering the riser was required before undertaking the experiments, given their scale. This was provided by using the commercial CFD package Star-CCM+ (version 15.04.010) to predict the flow regime type, and additionally provide an indication of the slug length, velocity, and frequency.

2.1.2.1. Governing equations. The turbulence model used in this investigation was the k-ω SST (Menter) model where SST stands for Shear-Stress Transport. The advantage of this model is that it can be applied not only to the boundary layers near pipe walls but also to the bulk flow. It does this by utilising the capabilities of k-ω in near wall boundary layer regions and applying the k-ε model for the bulk flow (Menter, 1994). Turbulence modelling is shared by both phases, so there is only one set of equations to be solved for turbulence modelling.

In this multiphase CFD analysis, a liquid and gas mixture is modelled using the volume of fluid method (VOF) (Hirt and Nichols, 1981). This method can be used to model the flow of two immiscible fluids, one continuous and the other dispersed. The continuous phase is modelled by a single set of continuity and momentum equations of the form (Mohmmed et al., 2020; Sadeghi et al., 2022):

$$\frac{\partial \overline{\rho}}{\partial t} + \overrightarrow{\nabla} \cdot \left(\overline{\rho}\overrightarrow{V}\right) = 0 \tag{3}$$

$$\frac{\partial}{\partial t}\left(\overline{\rho}\overrightarrow{V}\right) + \overrightarrow{\nabla} \cdot \left(\overline{\rho}\overrightarrow{V} \otimes \overrightarrow{V}\right) = -\overrightarrow{\nabla} p + \overline{\rho}\overrightarrow{g} + \overrightarrow{\nabla} \cdot \frac{\leftrightarrow}{\tau} + \overrightarrow{F}_{ST} \tag{4}$$

where the stress tensor, $\frac{\leftrightarrow}{\tau} = \overline{\mu}(\overrightarrow{\nabla}\overrightarrow{V} + \overrightarrow{\nabla}\overrightarrow{V}^{T})$ in Eq. (4), with the transpose denoted by the superscript, T. The volume fractions of the liquid (α_l) and gas (α_g) sum to unity. They are used to define the local average density ($\overline{\rho}$) and viscosity ($\overline{\mu}$) of the fluid by calculating a weighted average based on the volume fractions ($\alpha_{l,g}$) and values of the phase densities ($\rho_{l,g}$) and viscosities ($\mu_{l,g}$) respectively. This is defined in the following relations:

$$\overline{\rho} = \alpha_l \rho_l + \alpha_g \rho_g \tag{5}$$

$$\overline{\mu} = \alpha_l \mu_l + \alpha_g \mu_g \tag{6}$$

The continuum surface force model (Brackbill et al., 1992) is used to calculate the interfacial surface tension, $\overrightarrow{F}_{ST}$ in Eq. (7) as a volumetric force. This is determined from the curvature, κ, the normal vector to that curve at the interface, and the surface tension coefficient, σ as follows:

$$\overrightarrow{F}_{ST} = \sigma\kappa\overrightarrow{\nabla}\alpha_g \tag{7}$$

$$\kappa = -\overrightarrow{\nabla} \cdot \frac{\overrightarrow{\nabla}\alpha_g}{\left|\overrightarrow{\nabla}\alpha_g\right|} \tag{8}$$

Due to the sharp change from 1 to 0 anticipated for the volume fraction at the interface between the two fluids, a specific treatment is required to resolve this issue because simple higher order schemes would fail. This is accomplished in Star-CCM+ (15.04.010) using the High-Resolution Interface Capturing scheme (Mahrenholtz and Markiewicz, 1999) which is based on a normalised variable diagram. This requires calculation of the normalised face value, ξ_f from the normalised cell value of the donor cell, ξ_c:

$$\xi_f = \begin{cases} \xi_c \ if \ \xi_c < 0 \\ 2\xi_c \ if \ 0 \le \xi_c < 0.5 \\ 1 \ if \ 0.5 \le \xi_c < 1 \\ \xi_c \ if \ 1 \le \xi_c \end{cases} \tag{9}$$

The value determined by this equation is further modified by using the local Courant number, *Co* to prevent discontinuity problems occurring. The availability criterion is used for this process, with an upper (Co_u) and lower (Co_l) value for *Co* being used. This dictates that the maximum amount of a fluid available in any given timestep must be less than or equal to that in the donor cell. To achieve this, the following correction is applied:

$$\xi_f^* \begin{cases} \xi_f \ if \ Co < Co_l \\ \xi_c + (\xi_f - \xi_c)\dfrac{Co_u - Co}{Co_u - Co_l} \ if \ Co_l \le Co < Co_u \\ \xi_c \ if \ Co_u \le Co \end{cases} \tag{10}$$

To enable smooth switching between schemes, a final correction is made to the normalised face value based on the angle, θ, between the normal to the interface and the cell-surface vector. The default value for the angle factor, C_θ , is 0.05. The correction is applied using:

$$\xi_f^{**} = \xi_f^*(\cos\theta)^{C_\theta} + \xi_c\left(1 - (\cos\theta)^{C_\theta}\right) \tag{11}$$

Since the two-phase slug flow is time dependent, an implicit unsteady solver was used with a timestep, $\Delta t = 0.0005s$. A total physical time of 30 s was employed to allow the slug flow to develop and stabilise. This timestep, in conjunction with the cell size, permitted the Courant number to be kept below 0.25 to minimise numerical diffusion (Ratkovich et al., 2013).

2.1.2.2. Grid independence. A generalised cylinder mesh with a series of prism layers at the wall was used to discretise the domain. This mesh type was designed to deal with flows inside pipes, which is what is being modelled in this case. Additionally, since this mesh is orthogonal, it is in keeping with recommendations for mesh types to use in simulations of two-phase flow (Hernandez-Perez et al., 2011).To determine the grid independence of the mesh, a series of meshes were generated with cell counts of 522,000, 653,000, 872, 000, 1300,000, 1700,000, 2200,000 and 2600,000 cells. The liquid holdup was monitored on a circular cross section at 10 m from the inlet for all meshes, which were run for 30 s of physical time. This time was more than sufficient to allow slug generation and transit through the entire domain. Since slug development must occur prior to the initial time chosen, in all cases, slugs had developed by the passage of 10 s of physical time. This time was chosen as the initial point for measurement. To create a benchmark, this time must be consistent for all grid sizes. As such, a 10 second period of time was chosen, as this was sufficient to permit a significant number of slugs to pass through the domain and thereby determine the slug frequency for comparison. The mean slug frequency was determined for the number of slugs over the 10 second period between 10 and 20 s of physical time for a flow with $U_{sl} = 2.0\, ms^{-1}$ and $U_{sg} = 0.75\, ms^{-1}$. A significant difference in slug frequency was observed between 522,000 cells and 1300,000 cells but increasing the cell count to 2.6 million cells produced no appreciable difference, as shown in Fig. 2 below. Based on this result, the mesh of 1.3 million cells was chosen as a good balance between computational load and accuracy.

2.1.2.3. Computational domain. The computational model geometry was set up as shown in Fig. 3a. As in the PETEX GAP simulations (Section 2.1.1), the riser was modelled as a rigid structure and the same quarter ellipse geometry was applied for the purposes of predicting flow regimes, as shown in Fig. 3. Downstream of the riser section, the piping to the return loop was originally planned to traverse vertically through the clear viewing section with a short (830 mm) additional vertical section (see Fig. 3a). Following, this a 90° bend would take the flow horizontally for approximately 1 *m* before a second 90° bend sent the flow downwards vertically once more, leading to the return loop to the separator (as shown in Fig. 3a). During the build, however, this design proved not to be possible at the host facility, so the second 90° bend took the flow horizontally in the z-direction instead (as shown in Fig. 3b). This did not change the riser configuration and was considered to be far enough from the inlet of the riser, which was the part of greatest interest, to have significant effect on the flow in the riser. With regards to the upstream section of the geometry, it was known that over 10 *m* of development section was available and that there would be a section of 6″ piping leading into the 2″ section. The respective lengths and

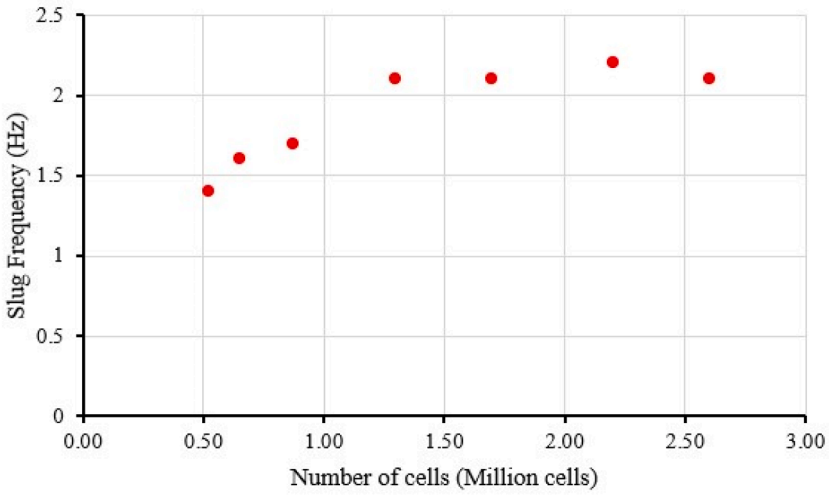

Fig. 2. Grid Independence analysis for CFD.

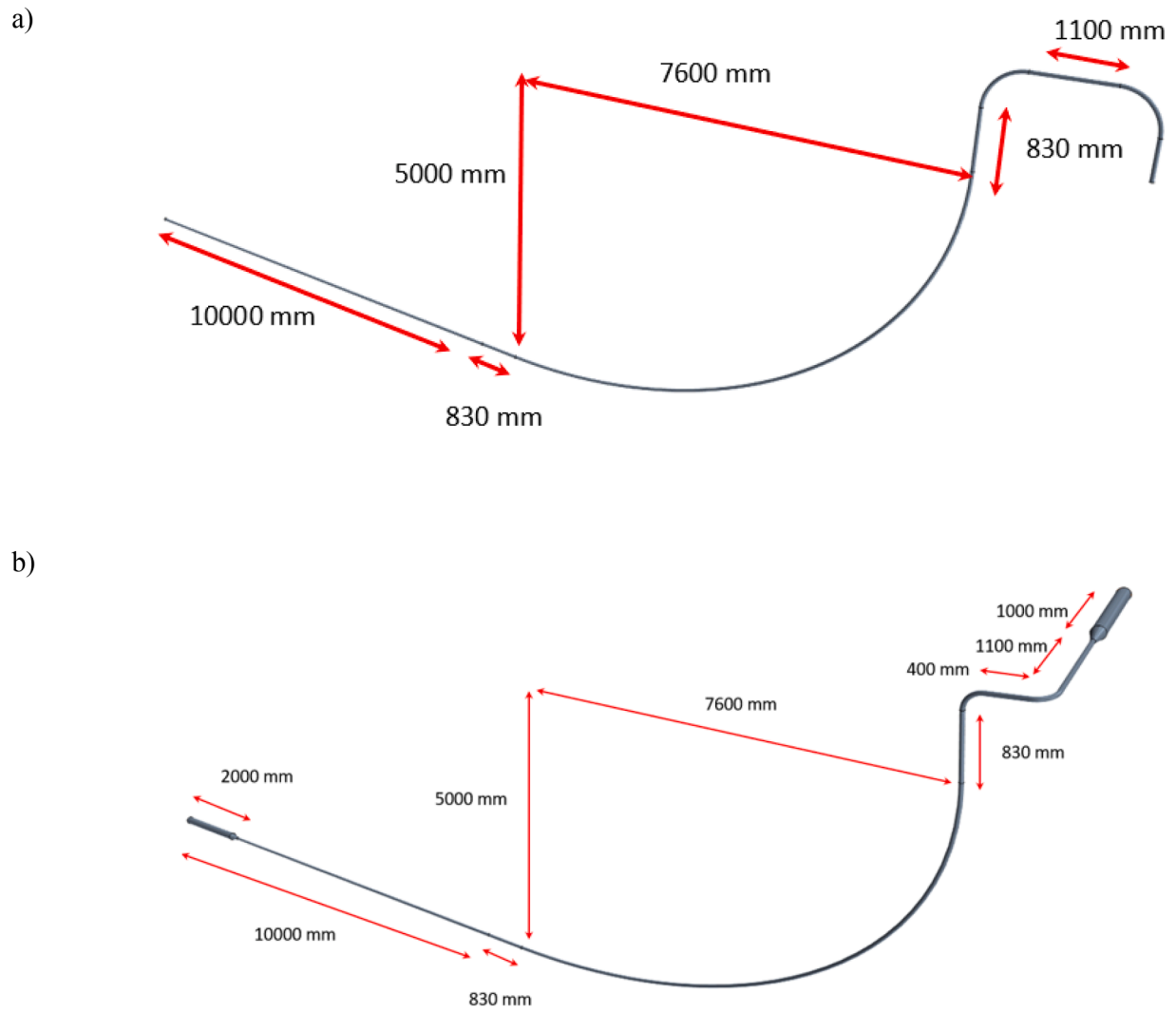

Fig. 3. a) Initial geometry used for investigation of flow regime using CFD, b) actual geometry from experiment.

reducers forming this change in internal diameter were not determined at the time the CFD model was designed. As a result, the geometry was designed with 10 m of 2″ pipe. Given that in the experiment, the 2″ straight development section would be preceded by a length of 6″ piping, it was concluded that a flat stratified inlet condition would not be a realistic representation.

As such, a sinusoidal wave function was applied at the inlet to introduce an unsteady interfacial surface between the two phases and so define the free surface level of the liquid phase as a function of time (Al-Hashimy et al., 2016, 2015; Frank, 2005):

$$y_1 = y_0 + A_1 \sin\left(2\pi \frac{U_{sl} t}{p_1}\right) \tag{12}$$

where, y_1 is the height of the water fraction on the inlet, $y_0 = 0$, $A_1 = 0.0127m$, $p_1 = 3m$, and U_{sl} is the liquid superficial velocity, which varies from test point to test point. The amplitude of this perturbation, A_1, was set to one quarter of the internal diameter of the pipe. By setting $y_0 = 0$, the height of the water fraction in this sine function was based upon the centreline of the pipe. This generates a sinusoidal variation in height of the water volume fraction at the inlet as a function of time. The wavelength, p_1, was set to approximately one third of the total length of the development section in order for the fluctuations imposed to have minimal effect over the ensuing slug flow characteristics. It is worth noting that this perturbation of the inlet condition was not the cause of the slug flow. Once the test points were determined as described above, additional tests using a stratified inlet condition were conducted, which also produced slug flow at the riser inlet.

2.2. Final test matrix

Simulations were conducted on the test point matrix that PETEX GAP modelling had indicated would produce slug flow at the inlet of the riser. An additional number of test points were rejected based on the CFD simulation results. Those failing to produce a satisfactory slug flow were excluded. Finally, a test matrix of ten multiphase test points (MP1–10) was produced with confidence that they would yield a slug flow in the experiment. Additionally, a series of single-phase (nitrogen) test points (SP1–4) were produced at corresponding gas flow rates to those of the multiphase test points. This was done to establish how the pipe vibrated when under the influence of single-phase flow. Finally, test points (TP1–3), which were intended to be part of the testing but were unable to be run due to safety reasons, have been included for completeness (see Section 4.2.2 and Fig. 19). A summary of the gas flow rates and liquid flow rates which were investigated is shown in Table 1.

The locations of the test points on the flow regime map are shown in Fig. 4. The tests were designed to be run in the first instance with a constant liquid flow rate while varying the gas flow rate in order to ascertain the effect of increasing gas flow rate had upon the response of the flexible riser section. This is indicated in Fig. 4 by the purple arrow indicating the order in which the test points MP2, MP5, MP6, and MP3 were executed. On completion of this, the gas flow rate was kept constant while the liquid flow rate varied such that a similar understanding could be obtained with decreasing liquid flow rate. The red arrows in Fig. 4 following the test points MP3, MP7, MP8, MP9, and MP10 are used to show this.

3. Experimental methodology

To assess the effect nitrogen/water slug flow has on the structure of a flexible Riser, a 10 *m* long MERLETT Vacupress Cristal hose was installed in the AMF. The AMF is a closed loop, multi-phase test facility offering a combination of oil (Exxsol), saline water and gas (Nitrogen). The flow rate of oil can be varied between 0.2 m^3/h - 550 $m^3/h \pm 0.5$ %, that of saline water between 0.2 m^3/h - 550 m^3/h $\pm$ 0.5 % and that of nitrogen between 8 Am^3/h (actual cubic meters at current operating conditions) to 3000 $Am^3/h \pm 1$ %, at operating pressures between 10 Barg and 140 Barg. Only water and nitrogen were used for the experiments here. Upstream of the test section, the multiphase flow is combined using a custom-built mixing manifold, which is located approximately 13.5 m upstream of the 6″–2″ reducer shown in Fig. 1. Downstream of the test section, the flow is separated back out into its constituent components using a custom separator. The separated components are then fed back into the supply loop upstream of the test section. The AMF forms part of the UK's National Measurements Institute responsible for the management of the UK standards for flow measurements ("GOV.UK 2022). The PVC hose had a 0.9 mm thick galvanised steel spiral (Youngs modulus, $E = 200$ GPa, Poisson's ratio $\mu \approx 0.3$) embedded within it and was reinforced with a woven polyester yarn with a weave strand thickness of 0.8 mm. The pipe had a nominal ID = 50.8 mm, a burst pressure of 30 barg, a minimum bending radius of 170 *mm* and weighed 1.6 *kg/m*. The pipe was a composite structure with a non-uniform cross section as shown in the simplified schematic diagram of the pipe shown in Fig. 5. Values given in Fig. 5 are from measurements manually taken on the actual pipe used in the experiment. Stainless steel ASA150 flanges attached to both ends of the pipe allowed it to be hung freely between the rigid sections of the AMF test loop. The riser had a vertical drop of 5 m and a horizontal travel of 7.7 *m*. Upon pressurisation, the pipe extended in length therefore to prevent sagging of the pipe, the first 2.3 *m* of the pipe was secured to a rigid horizontal support. This increase in length was due to the embedded steel spiral, which was able to extend in an axial direction (due to the pressure differential between the interior of the pipe and the surroundings), but not transversally. This ensured that this section of the pipe did not move and that the vertical drop and horizontal distance of the hose were not affected. A schematic diagram of the test rig installed in the AMF is shown in Fig. 1. The AMF has a maximum gas flow rate of 3000 m^3/hr and a maximum liquid flow rate of 550 m^3/hr which determined the minimum flow rate for the tests, as mentioned in Section 2.1. For the purposes of this investigation, a mixture of nitrogen and water was used to generate the slug flow. A summary of the physical properties of the

Table 1
Gas and liquid flow rates and associated superficial velocity for single and multiphase test points.

Test Point Number	Gas flow rate m^3/hr	Liquid flow rate m^3/hr	Gas superficial velocity ms^{-1}	Liquid superficial velocity ms^{-1}
SP1	18.3	0	2.5	0
SP2	9.6	0	1.3	0
SP3	7.3	0	1.0	0
SP4	5.5	0	0.75	0
MP1	7.3	10.9	1.0	1.5
MP2	5.5	14.5	0.75	2.0
MP3	18.3	14.5	2.5	2.0
MP4	5.5	10.9	0.75	1.5
MP5	7.3	14.5	1.0	2.0
MP6	9.6	14.5	1.3	2.0
MP7	18.3	5.5	2.5	0.75
MP8	18.3	4	2.5	0.6
MP9	18.3	3	2.5	0.4
MP10	15	3	2.0	0.4
TP1	9.6	22.1	1.3	3.0
TP2	5.5	29.1	0.75	4.0
TP3	18.3	29.1	2.5	4.0

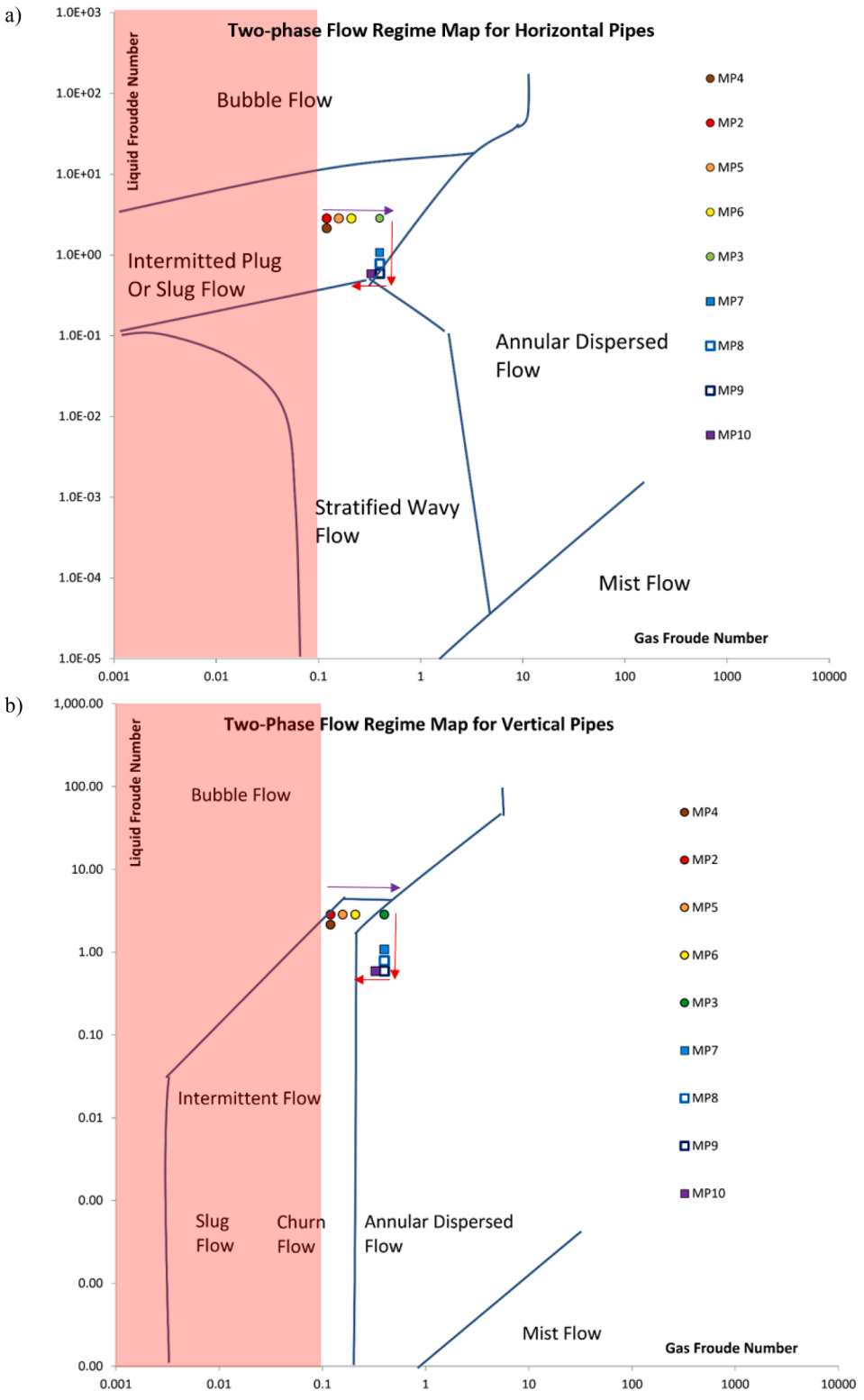

Fig. 4. Shell flow regime map showing test points for a) horizontal flow and b) vertical flow. Red area indicates excluded zone.

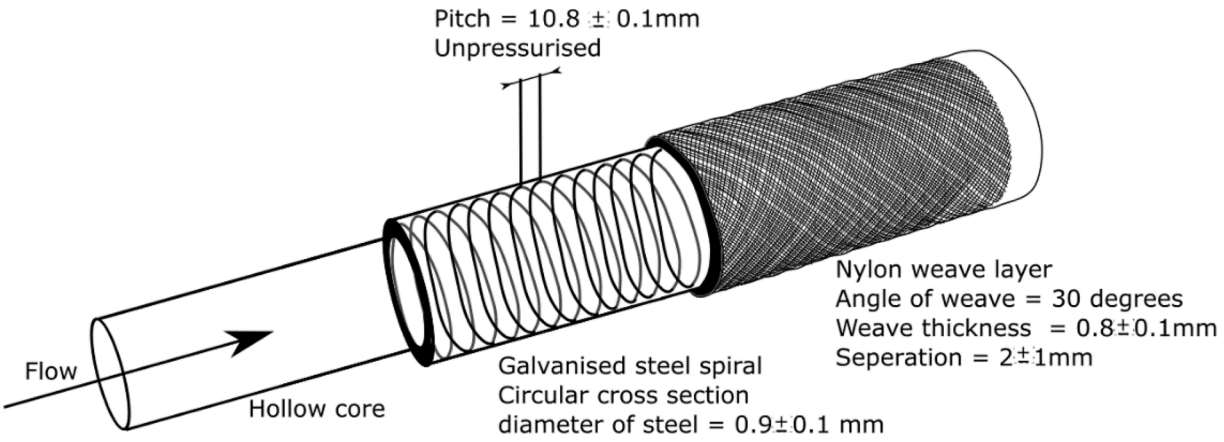

Fig. 5. Schematic diagram demonstrating the non-uniform structure of the pipe.

Table 2
Material properties of working fluids with the corresponding measurement accuracy as provided by the facility's operator.

Fluid	Density (ρ) kgm^{-3}	Dynamic viscosity (μ) $Pa\ s$	Surface Tension (σ) Nm^{-1}
Water	1041 ± 0.3	1.18 ± 0.025	0.072
Nitrogen	13.67 ± 0.285	0.018 ± 0.000045	–

fluids used in this investigation are presented in Table 2. The gas flow rate, Q_g was varied from 5.5 m^3/hr to 18.25 m^3/hr and the liquid flow rate, Q_l was varied from 0 to 14.5 m^3/hr. A summary of the various gas flow rates and liquid flow rates investigated is shown in Table 1 (Section 2.2).

The following procedure was used to transition through the selected test points. The gas flow rate was gradually increased from 0 m^3/hr to 5.5 m^3/hr with zero liquid inside the pipe (SP4). After which, whilst maintaining a gas flow rate, Q_g of 5.5 m^3/hr, the liquid flow rate was increased from $Q_l = 0$ m^3/hr to 14.5 m^3/hr (SP4 → MP4 → MP2). This allowed the effect of increasing the liquid flow rate whilst maintaining the gas flow rate to be investigated. Once a liquid flow rate of $Q_l = 14.5$ m^3/hr had been reached, the gas flow rate was gradually increased from Q_l of 5.5 m^3/hr to 18.25 m^3/hr (MP2 → MP6 → MP3). Unfortunately, excessive movement of the pipe, and the subsequent forces experienced by the support structure meant that increasing the gas flow rate above $Q_g = 18.25$ m^3/hr, in multiphase flow was deemed unsafe. In order to ensure that the test procedure selected did not affect the results obtained, test points were then repeated by transitioning between different test points. A summary of the testing procedure is shown in Table 3.

The pressure was measured at various points along the test loop. The frequency of the pressure measurements at each of the points within the test loop was 1.0 Hz. However, the average pressure upstream of the test section, at the position shown in Fig. 1 as P_r was considered to be the reference pressure for the system. This averaged to be 10.84 ± 0.15 (standard deviation) *barg* over all flow regimes investigated. The local averaged pressure at the entrance and exit of the riser, (P1) and (P2) respectively allowed measurements of the average pressure drop caused by the flexible pipe for each of the test points to be determined. The location of the pressure tappings are shown in circular insets in Fig. 1. The 1.0 Hz sampling frequency of the pressure measurement system was not sufficient to allow features within the pressure signals to be accurately determined given the slug frequencies that were experienced. A Cartesian (x,y,z)-coordinate system, with its origin at the geometric centre of the hose at the flange outlet plane at the bottom of the hose, is defined so that y-axis is vertically upwards, and the x-axis is orientated with the direction of the flow at this location.

To measure the movement of the pipe, three single axis PCB:352C22 ICP accelerometers were attached to the pipe at specific locations as shown in Fig. 6. Two accelerometers, AC1 and AC2, were mounted on top of the pipe, $x/ID = 35.3$ and $x/ID = 50$ from the flange outlet plane at the bottom of the hose respectively. A third accelerometer (AC3) was positioned on the side of the pipe to measure the out of plane movement in the positive z-axis, $x/ID = 35.3$ from the flange outlet at the bottom of the hose. The data from all three accelerometers were acquired, simultaneously, over a period of 20 mins with a data acquisition rate of 1600 *Hz*.

Table 3
Test sequence.

Sequence Number	Order of test procedure
1	SP1→SP2→SP3→SP4
2	SP1→MP4→MP2→MP5→MP6→MP7
3	SP4→MP4→MP2→MP5→MP6→MP3→MP6→MP5→MP7
4	SP4→MP4→MP5→MP7
5	SP4→MP10→MP11

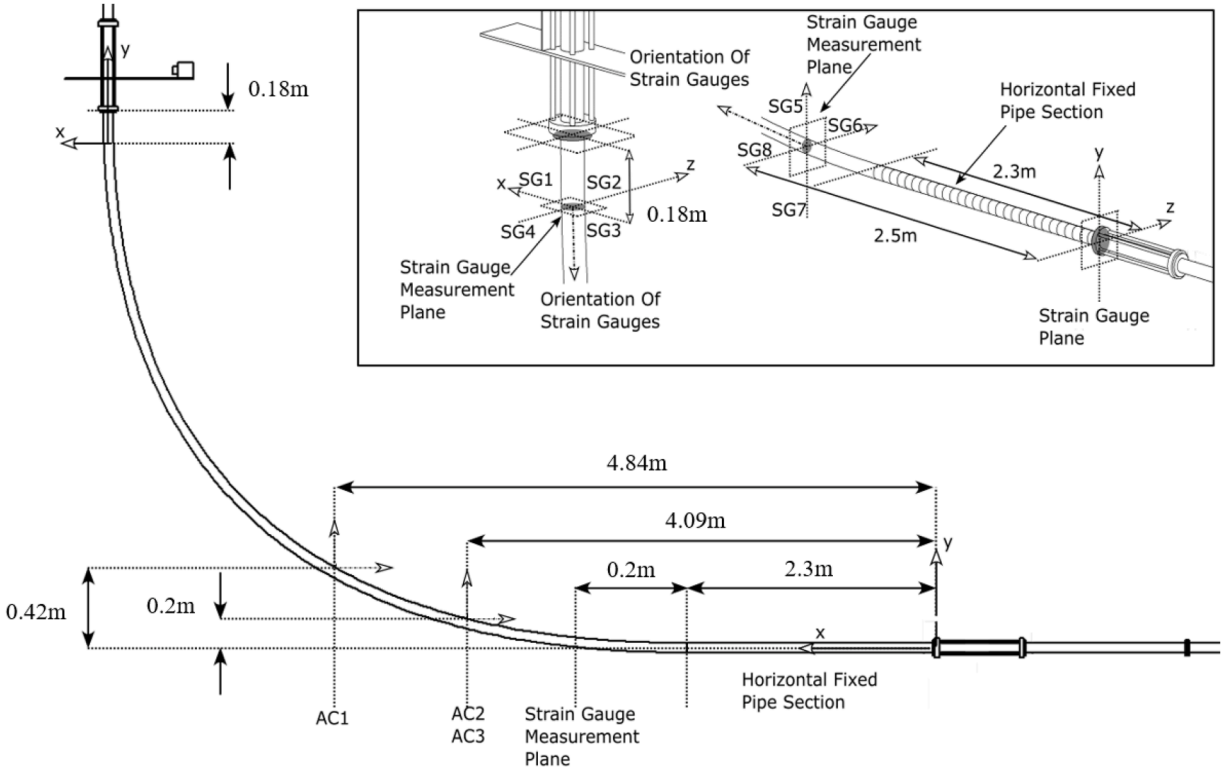

Fig. 6. Schematic of positioning of strain gauges and accelerometers with respect to the fixed flange positions with position and orientation of strain gauge planes and positions (inset).

A set of four axially aligned, Youmile BF120–3AA, 120 Ohm strain gauges were mounted onto the surface of the pipe 2.5 *m* from the flange outlet plane at the bottom of the riser. The four strain gauges were equidistantly distributed around the perimeter of the pipe (SG 5,6,7,8). A second set of strain gauges were also mounted, axially, to the surface of the pipe 3.5 *ID* before the end of the flexible hose (SG 1,2,3,4), as shown in Fig. 6 (inset). The data from all eight accelerometers were acquired simultaneously, over a period of 20 min per test point with a data acquisition rate of 1562 *Hz*. It should be noted that the strain gauges were installed after the pipe had been pressurized to prevent them from being damaged when the pipe deformed during pressurization. At the beginning of each day of testing, the null offset was applied to each of the strain gauges. This was performed when the pressurized pipe was hanging freely with zero gas flow rate and zero liquid inside of the pipe.

In order to visualise the flow inside the pipe, custom PVC sections were installed at both the top and bottom of the flexible riser, as shown in Figs. 1 and 6. Upstream of the flexible riser, a Photron FASTCAM SA1.1 high speed, 1 megapixel camera with a 1024×1024-pixel CMOS sensors fitted with a Nikon AF Nikkor $24 - 85$ *mm* focal length lens set to $f\# = 2.8D$ was used to record the structure of the flow entering the riser. This camera was positioned to record a 0.116 *m* section of the horizontal clear PVC pipe 2″ ID. Immediately after exiting the riser, in the vertical section of the test loop, a Photron FASTCAM Mini Ax digital high speed, 1 megapixel camera with a 1024×1024 pixel CMOS sensor fitted with a Nikon AF Nikkor 50 *mm* focal length lens set to $f\# = 1.8$, mounted to the observation section, using a custom mount, was used to acquire images of the flow as it left the riser. This camera was positioned to record a 0.123 *m* section of the vertical clear PVC pipe 4.6 ID from the end of the flexible riser ($y = 5.25$ *m*). Light diffuser boards and spotlights ensured that images recorded from both cameras were back lit and had uniform background light intensities. The cameras were both configured to record 10 sequences of 1000 images at 1000 fps, 120 *s* apart simultaneously, giving a total recorded time of 10 s for each test point investigated. The strain gauge data, accelerometer data and camera data were all triggered to start acquiring data within 12.5 *ns* using a custom data acquisition system based around a NI DAQ 9178.

For this investigation pressure measurements were also recorded at two locations along the test loop. Pressure tappings, P_1 and P_2, were located at the bottom and top of the flexible riser, respectively, and locations of the pressure measurements are shown in circular insets in Fig. 1. Unfortunately, the sampling frequency of this measurement system was not sufficient to determine features within the pressure signals; however, it was possible to obtain the average pressure drop across the flexible riser.

4. Results

The effect internal slug flow has on the movement of a flexible riser was characterised using accelerometers and strain gauges which were externally mounted to the riser. High speed cameras, pressure sensors and flow meters were used to access the conditions

of the flow inside the pipe immediately before and after the flexible riser. Firstly, results are presented for single-phase, (100 %) gas flow inside of the pipe. Subsequently, the results obtained when multiphase slug flow flows inside the flexible riser are presented.

4.1. Single phase gas flow

The mean absolute acceleration of the three accelerometers used to measure the movement of the flexible riser when the single-phase gas flow rate, Q_g was varied from 5.5 m^3/hr to 18.25 m^3/hr are shown in Fig. 7a). Under single-phase gas conditions, the vertical (AC1, and AC2) and horizontal (AC3) components of acceleration of the pipe's movement were of a similar magnitude. Integration of the accelerometers readings in the Fourier domain yielded the corresponding peak-to-peak displacements shown in Fig. 7b). For the single-phase gas flow rates investigated, the pipe did not move significantly as shown in Fig. 7b). The movement of the flexible riser led to the onset of axial strain at both the top and bottom of the riser.

As the single-phase gas flow rate Q_g was varied from 5.5 to 18.25 m^3/hr the mean axial strain experienced by the flexible riser is shown in Fig. 8a. It should be noted that the results obtained from SG8 were unreliable and therefore have been excluded from the results presented in this paper. It is believed that a loose connection, resulting from the movement of the pipe is responsible for this. The results show that for strain gauges SG1, SG4, SG7, the mean strain experienced by the pipe is approximately zero for all gas flow rates investigated. The mean strain experienced by coupled strain gauges (SG1-SG3, SG2-SG4 and SG5-SG7) is not symmetrically linked, indicating that the pipe deforms because of the movement of the pipe. The two stain gauges, SG3 and SG5, located on the nominal top side of the riser (see Fig. 6), were under significantly greater mean strain. Additionally, the two strain gauges on the right-hand side (as shown in Fig. 6) also underwent greater mean strain. Root mean square of the fluctuations (RMS), presented in Fig. 8, show that increasing the single-phase gas flow rate does not significantly affect the magnitude of the fluctuations at any of the measurement locations. Further, the single-phase gas flow is not seen to generate much in the way of variance in the strain measurements, with the variation in the RMS of the fluctuation of the strain being approximately an order of magnitude lower than the mean strain. The RMS of the fluctuation of the strain (Fig. 8b), indicates that for the top and right-hand side strain gauges, both the mean and the fluctuation in the strain were significantly higher than that observed in the other strain gauges. The average pressure drop produced by the flexible pipe for all of the single-phase test points was approximately 0.22 *bar*. As expected, when the pipe contained 100 % gas, the cameras installed either side of the flexible riser did not identify any flow features and therefore are not presented here.

4.2. Multiphase flow

4.2.1. High-Speed camera imaging

Visualisation of the flow inside of the pipe before it entered the flexible riser was performed in order to determine the structure of the flow entering the riser. Post processing of the videos, completed in MATLAB, allowed the flow entering the riser to be characterised. A flow chart illustrating the video data post processing pipeline that was used to extract slug parameters such as gas slug length, S_g, liquid slug length, S_l (see Fig. 8), and averaged gas slug frequency, S_f, from the videos is shown in Fig. 9(Matamoros et al., 2014; Mayor et al., 2007; Widyatama et al., 2016). An example of the structure of the flow entering the riser for each of the multiphase test points investigated is shown in Fig. 10. Inversion of the raw images allowed slugs to be identified more efficiently. This technique assumes that the slug velocity (for each test point) is constant, which holds when the bubble is neither coalescing, interacting with another

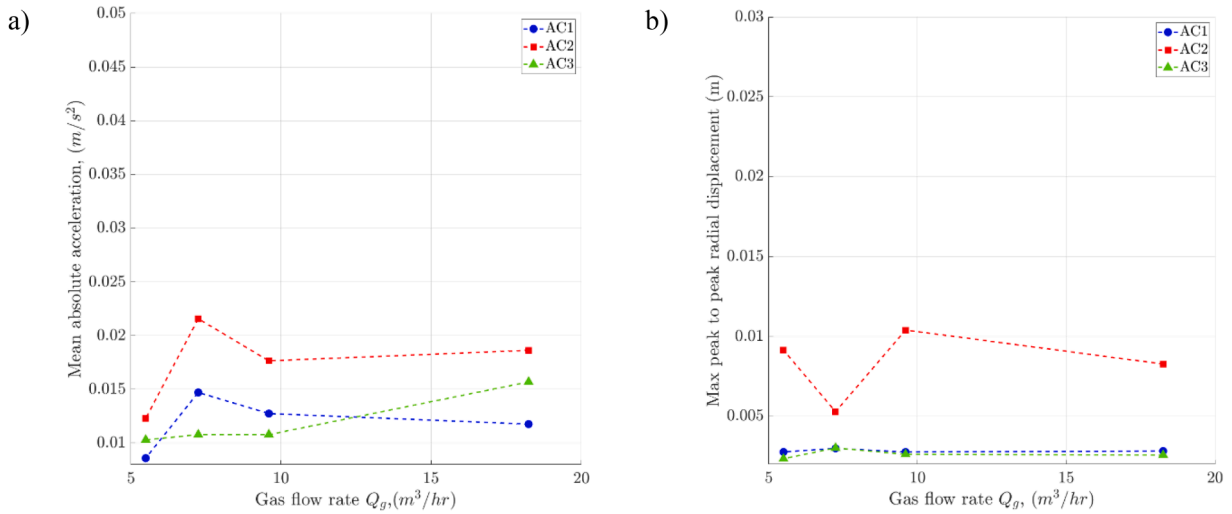

Fig. 7. Showing a) mean absolute accelerations and b) maximum peak to peak radial displacement of the flexible riser when the single-phase gas flow rate was varied from $Q_g = 5.5$ to 18.25 m^3/hr.

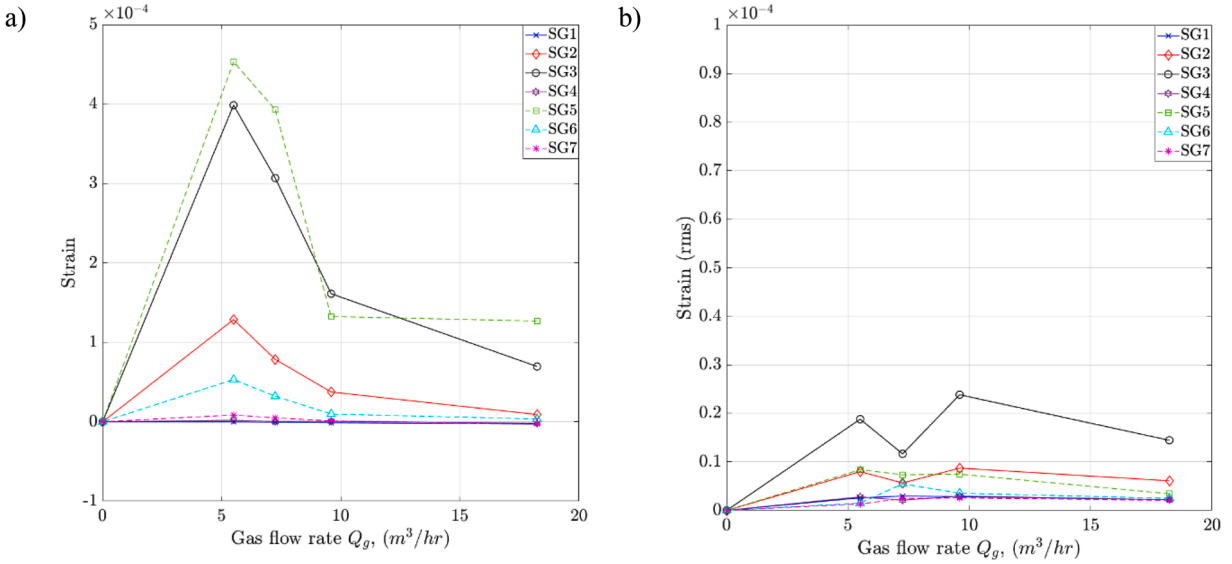

Fig. 8. a) mean strain gauge values and b) the RMS of the fluctuations of the strain experienced by the flexible riser when the single-phase gas flow rate was varied from $Q_g = 5.5$ to 14.5 m^3/hr.

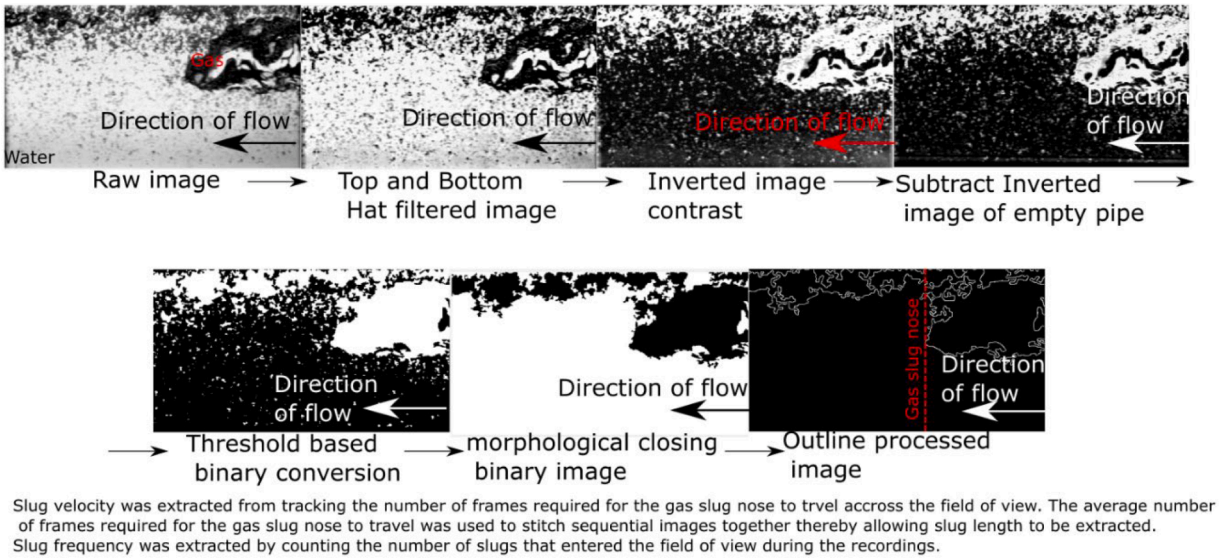

Fig. 9. An example of the video data processing pipeline, defined by Widyatama et al. (2016) used to extract slug parameters such as velocity, length and frequency from the high-speed recordings. .

bubble, nor instantly accelerating/decelerating (Mayor et al., 2007).

Table 4 contains observations of the flow field and, where applicable, the mean slug length, the variance of the slug length and the averaged slug frequency of the flow entering the riser for each test condition investigated. Analysis of Table 4 shows that the flow conditions entering the pipe matched the flow conditions predicted by both the CFD and the PETEX GAP investigations described earlier. Unfortunately, for a gas flow rate of 15.0 m^3/hr and a liquid flow rate of 3.0 m^3/hr (MP10), the size of the gas slugs was very large, meaning the lengths of the slugs could not be extracted from the videos recorded.

Further, for some of the test points there was intense gas entrainment in the liquid slugs and the curvature of the pipe rendered accurate measurement of some slug parameters impossible.

As the gas flow rate was increased (MP2, MP5, MP6, and MP3), there was a general increase in the gas slug length with MP2, MP5 and MP6 having lengths of 0.478, 0.657, and 0.880 m, respectively, with the standard deviation being approximately half the mean (see Table 4). The trend halted at MP3, with a mean slug length of only 0.164 m with a standard deviation of approximately five times the mean slug length. However, it is speculated that the intense fluid-structure interaction observed at this flow rate (see Section 4.2.2

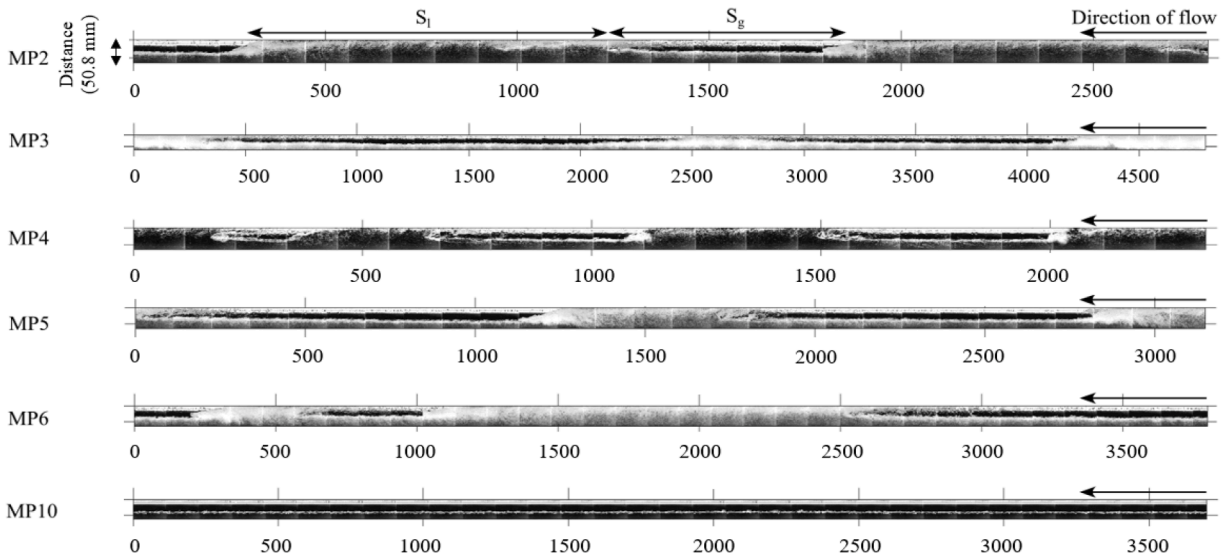

Fig. 10. Reconstruction of flow entering the riser showing gas slug length S_g and liquid slug length S_l parameters. The reconstructions shown represent 1 second of flow entering the riser and were recorded at 1000fps.

Table 4
Statistics of slugs entering the riser measured experimentally, extracted from processing 10 sequences of 1 s of the flow entering the riser, at a frame rate of 1000fps.

Test Point	Averaged gas slug length S_g (*m*)	Standard deviation of gas slug length (*m*)	Averaged gas slug frequency (*Hz*)	Averaged liquid slug length S_l (*m*)	Standard deviation of liquid slug length (*m*)
MP1	–	–	2.5	–	–
MP2	0.478	0.233	3.17	0.622	0.346
MP3	0.164	0.827	–	0.710	0.642
MP4	0.521	0.256	2.85	0.449	0.281
MP5	0.657	0.321	2.44	0.703	0.374
MP6	0.880	0.450	2.16	0.766	0.459
MP10	>3.861	–	0.375	0.363	0.155

and Figs. 18 and 19) may have affected the slug flow characteristics. The possibility of breaking up the slugs into small sizes with a much wider variation than seen in the other flows is then considered. With regards to the liquid slug statistics, the variation in slug length is less than that for the gas, but the trend is still observed as a general increase. Again, the standard deviation is approximately half the magnitude of the mean with the lone exception being MP3. While the comparison is not as stark as in the gas slug statistics, the mean slug length is again smaller than would be expected should the increased length trend continue. Additionally, the standard deviation is the greatest of all test points for the liquid slugs.

While some correlation was obtained between slug parameters produced in the experiment, and the values obtained from either CFD or PETEX GAP prior to the experimental campaign there was significant disagreement between them. Examination of the averaged liquid slug lengths determined using CFD (see Table 5) show that in only a couple of cases the CFD produced similar results to the experiments, namely, MP2 and MP4. Interestingly the standard deviation for all bar MP3 and MP6 was approximately half the value of the average slug length in agreement with the experimental results. The averaged gas slug lengths were less well predicted in all cases and showed comparatively lower values for standard deviation. The influence of the movement of the flexible riser section on the slug parameters at the entrance to said section is believed to be primarily responsible for this. Undulating motion was a key feature

Table 5
Statistics of slugs entering riser from CFD.

Test Point	Averaged gas slug length S_g (*m*)	Standard deviation of gas slug length (*m*)	Averaged gas slug frequency (*Hz*)	Averaged liquid slug length S_l (*m*)	Standard deviation of liquid slug length (*m*)
MP1	1.93	0.48	1.5	0.35	0.19
MP2	0.83	0.25	2.1	0.55	0.31
MP3	3.76	0.37	1.3	0.3	0.24
MP4	1.28	0.38	1.4	0.6	0.26
MP5	1.40	0.88	2.2	0.13	0.04
MP6	1.64	0.02	1.3	1.14	0.20

of the flexible pipe under experimental conditions and such motion, which was not modelled in either CFD or PETEX GAP, would encourage the break-up of large gas slugs that the rigid pipe simulation predicts. The complex interaction between the fluid and the pipe, whereby the motion and shape of the pipe affect the flow features, and the coupled effect of the flow feature's ability to influence the form and movement of the pipe, means that rigid structure modelling has limitations in its ability to predict flow features precisely. On the other hand, the rigid structure modelling was able to predict the flow regime successfully, if not the exact flow statistics for all test points investigated.

With regards to the images obtained from the camera mounted at the top of the riser, observing via the vertical clear section, there was a marked difference in the flow. At first sight, the flow appears to have devolved into a churn flow, though this may be misleading. Determination of any flow statistics for the vertical section, such as those in Table 4 for the horizontal section, was not possible. Insight into the actual flow type was obtained via two separate observations. Firstly, the riser pipe itself was only semi-transparent, which is what necessitated the use of the clear viewing sections, but it was possible to observe the slugs transitioning into the riser from the clear horizontal section. When this occurred, a distinct dark patch in the pipe could be seen, though no precise details such as length etc. could be obtained from this. The dark patch could be observed travelling the full length of the riser, without devolving into churn flow, and entering the underside of the clear viewing section. A clear example of which is shown in Fig. 11 for test point MP10. This would seem to indicate that the gas slug remained intact up until that point. The second observation was provided by the CFD, which showed that the gas slug body could detach itself from the upper surface as the angle increased to the vertical. Additionally, in the CFD, a region of high-volume fraction of water can be seen surrounding the slug, as shown in Fig. 12d and e. This flow is not a pure sheet of water enclosing the slug, it contains patches of lower volume fraction of water, indicating areas filled with fine bubbles which could block the view of the gas slug from the outside and give the appearance of a churn flow. It must be noted that the exterior of the pipe does not generally obscure the interior flow features in the CFD. Examination of Fig. 12a shows the view of the exterior of the pipe in the CFD and can be readily compared to Fig. 12b, which shows a bisection of the pipe in the vertical xy-plane (see Fig. 6) revealing a slice of the interior. Clearly, the flow features present in the planar section are very much visible in the exterior view. There are differences though, which is to be expected, but these are not so extensive as to obfuscate the flow features on the interior. Attention is now drawn to Fig. 12d, where it is not readily apparent as to what flow features might be hidden behind the water and bubbles. This is not revealed until a vertical bisecting plane is applied, and the interior revealed in Fig. 12e. By way of comparison from the high-speed camera images from the upper camera viewing the vertical clear section, Fig. 12c shows a typical sequence of images of the flow before a slug enters from the riser section to the slug departing. This flow of water containing fine bubbles was the consistent flow type observed except during the passage of a gas slug. The flow shown in Fig. 12c is representative of the view observed as a slug passes through the vertical viewing section. The transition from bubbly to churn and back to bubbly flow can clearly be observed. This phenomenon was observed in all recording of the vertical section for all test point examined. For test point MP2, MP4, MP5 and MP6 the vertical flow regime map (see Fig. 4b) predicts intermittent flow. It is worthy of note that for test points MP3 (shown in Fig. 12c), and MP7 to MP10, the predicted flow regime was annular dispersed on the flow regime map. The flow is highly complex and was frequently seen to contain reversed flow of the liquid phase during these transitions. In addition, it is not readily apparent as to whether the flow is a churn flow of if the larger (than those shown in Fig. 12c) bubbles are obscuring a true slug bubble behind them in a similar fashion to that shown in Figs. 12d and e.

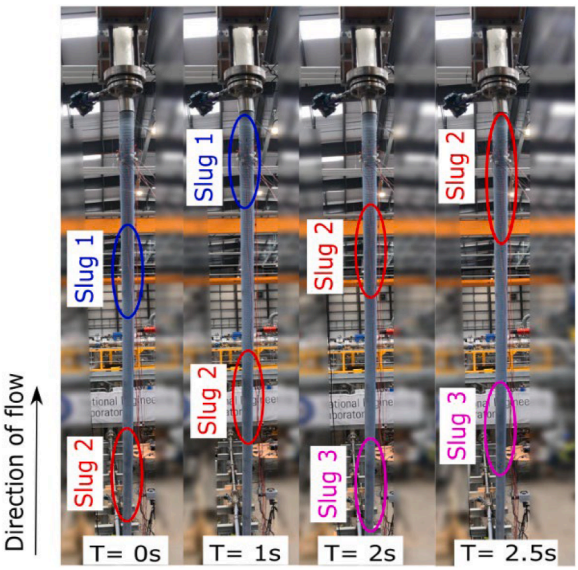

Fig. 11. Sequential images, taken from underneath the riser, showing the passage of the slug flow seen as dark patches along the pipe.

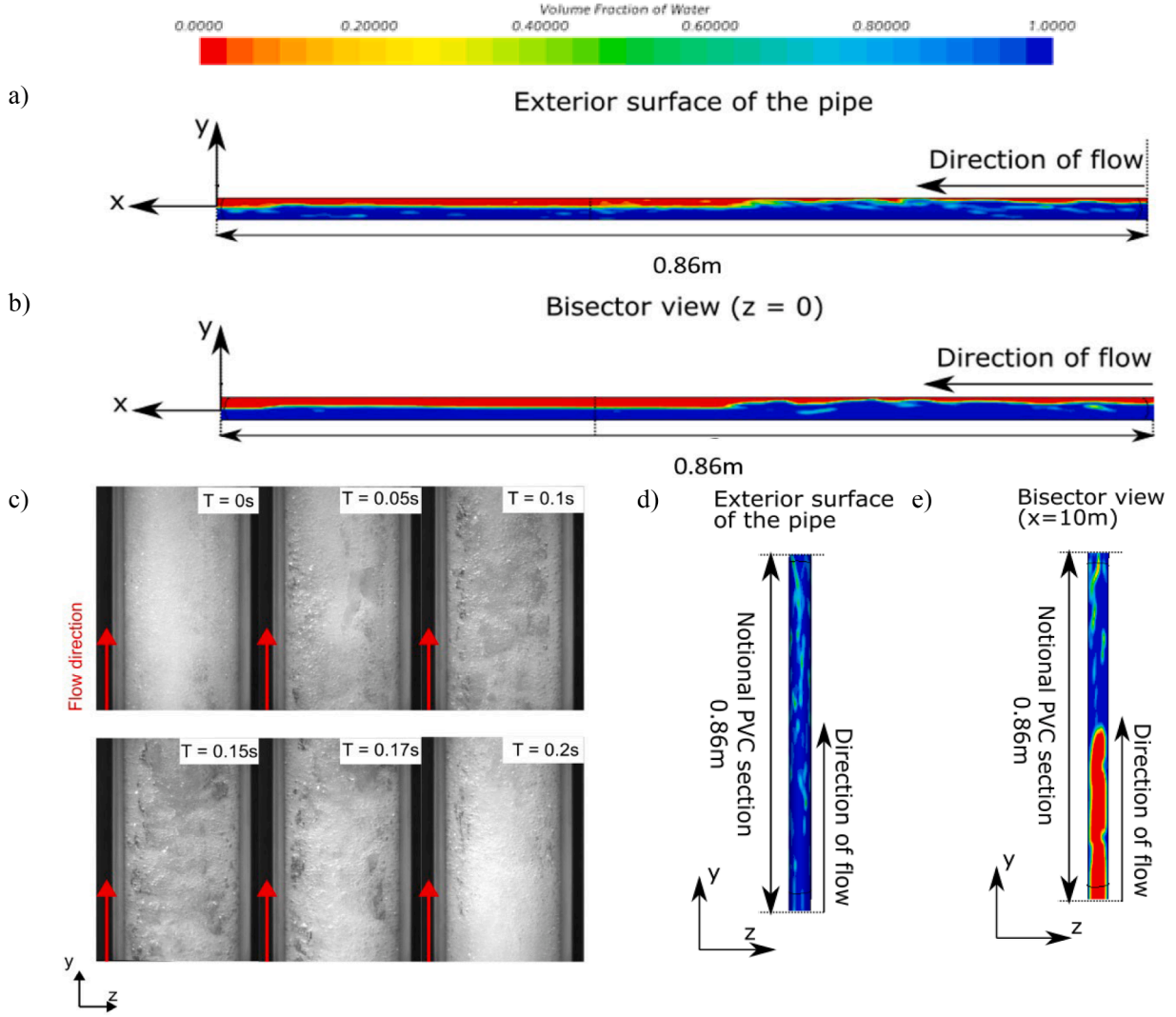

Fig. 12. CFD of the clear viewing sections showing the volume fraction of water at a) the outside of the pipe at the horizontal section, b) bisection in the xy-plane of the pipe at the horizontal section, c) experimental snapshots showing the variation of the structure of the flow leaving the riser d) the outside of the pipe at the vertical section, and e) bisection in the xy-plane of the pipe at the vertical section. All the images shown in this figure relate to the test point MP3.

4.2.2. *Movement of the pipe*

The mean absolute acceleration of the three accelerometers used to measure the movement experienced by the pipe when a constant gas flow rate, $Q_g = 18.25\ m^3/hr$ was applied and the liquid flow rate, Q_l was increased in steps from 0 m^3/hr to 14.5 m^3/hr is shown in Fig. 13. In this instance, a liquid flow rate of zero indicated a single-phase gas test point. The average acceleration values that the riser section experiences were approximately zero for all test points investigated. Fig. 13a shows a monotonic increase in the mean absolute acceleration, with an increase in liquid flow rate. This is likely due to the increased momentum associated with the increase in denser fluid phase. It is interesting to note that the mean absolute acceleration measured by the accelerometers mounted on top of the pipe (AC1 and AC2) were considerably larger than on the side of the pipe (AC3). This implied that the pipes motion was predominantly in the plane of the riser and that any out-of-plane motion was much less significant. This is supported by the results shown in Fig. 13b, which shows the peak to peak radial displacement of the pipe as the liquid flow rate was increased. The recorded maximum displacement in all multiphase flow measurements was an order of magnitude greater than that seen in single phase flow (see Fig. 7).

The converse of this procedure, whereby liquid flow rate was kept constant at $Q_l = 14.5\ m^3/hr$ and the gas flow rate was varied from $Q_g = 5.5\ m^3/hr$ to $18.25\ m^3/hr$ is shown in Fig. 14. Again, the averaged accelerations experienced by the pipe were approximately zero. Likewise, the acceleration experienced by AC1 and AC2 were significantly higher than those of AC3 as shown in Fig. 14a). Additionally, as shown in Fig. 14b) the displacement maxima indicated that the out-of-plane movement of the pipe was significantly smaller than its in-plane movement. Analysis of Fig. 14a) shows that, for a liquid flow rate of $Q_l = 14.5\ m^3/hr$, increasing the gas flow rate significantly increased the magnitude of the acceleration experienced by all three accelerometers. At lower gas flow rates, $5.5 \leq Q_g <$

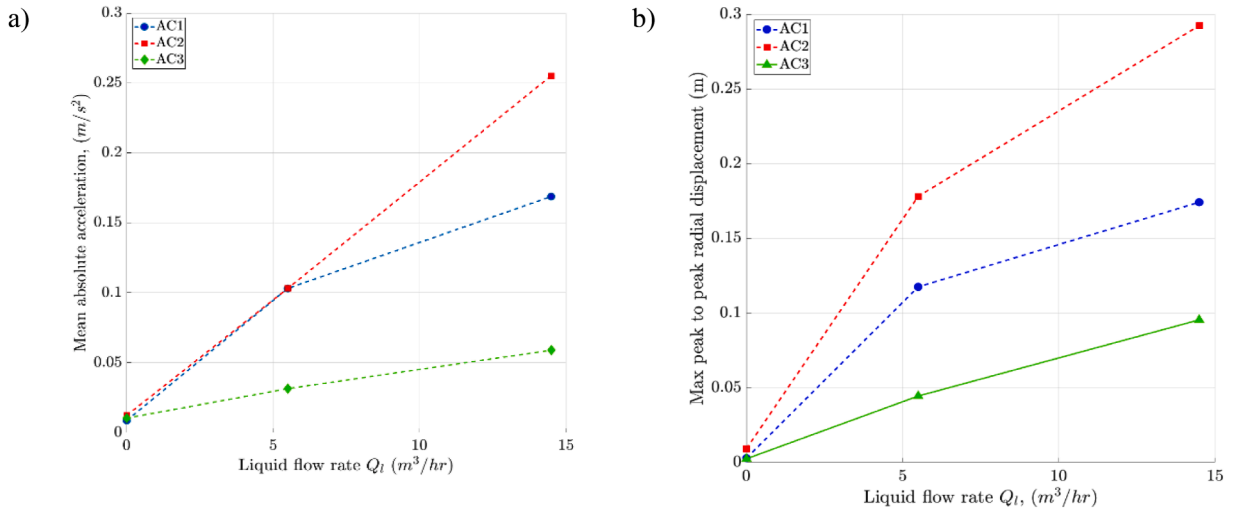

Fig. 13. Showing a) the mean absolute acceleration and b) the maximum peak to peak radial displacement of the flexible riser when the gas flow rate was kept constant, and the liquid flow rate varied.

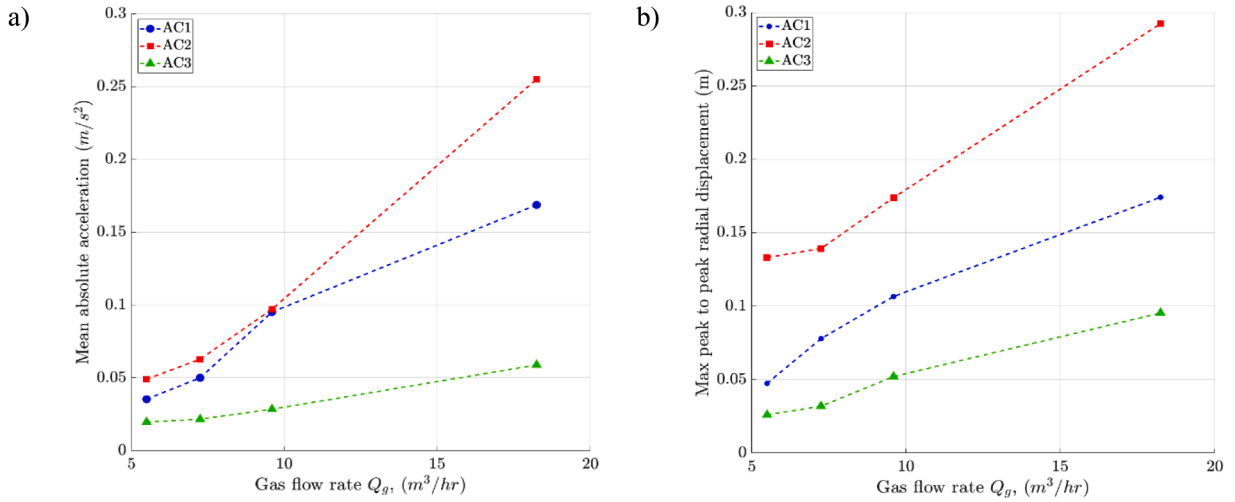

Fig. 14. Showing a) the mean absolute acceleration and b) maximum peak to peak radial displacement of the flexible riser when the liquid flow rate was kept constant, and the gas flow rate varied.

10.25 m^3/hr, the mean absolute acceleration experienced by AC1 and AC2 were similar in value; however, at a gas flow rate of $Q_g =$ 14.5 m^3/hr, the acceleration experienced by AC2 were noticeably larger than AC1. The same can be observed in Fig. 13.

The movement of the pipe generated strains in the flexible riser at the fixed connections with the flanges. Time histories of strain gauges (SG1-SG7), when the flow inside the pipe transitioned from test point SP4 to test point MP4 are shown in Fig. 15 (a-g) below. Analysis of Fig. 15 shows that when transitioning from single phase to multiphase flow, during the transient phase compression can be seen in some of the strain gauges (SG1, and SG7); however, further analysis of Fig. 15 shows that, after a transient period, all the strain gauges indicate that the pipe was under tension. It is theorized that the added weight of the water inside of the flexible riser caused the pipe to stretch thereby causing all of the strain gauges to give positive readings. This indicated that the pipe was under tension compared to when it was free hanging, pressurized and had zero flow inside of it. Fig. 15(h) also shows the response of SG5 and SG7 which were mounted on either side of the pipe. From Fig. 15(h) it is clear that whilst they are both indicating tension with regards to the free hanging, pressurized zero flow condition, the fluctuations about their respective mean strain values are opposing, indicating that as expected when one side of the pipe is under compression the other is under tension. It should be noted that, when transitioning between any of the other multiphase test points, the strain gauges did not indicate that the pipe was under compression when compared to the empty, free hanging, pressurized pipe. An example of which is shown in Fig. 16, which shows the time history of strain gauge SG4 as the flow inside the pipe transitioned from MP4 to MP2.

Fig. 17 shows the mean strain and the RMS of the fluctuations of the strain experienced by the flexible riser when the gas flow rate

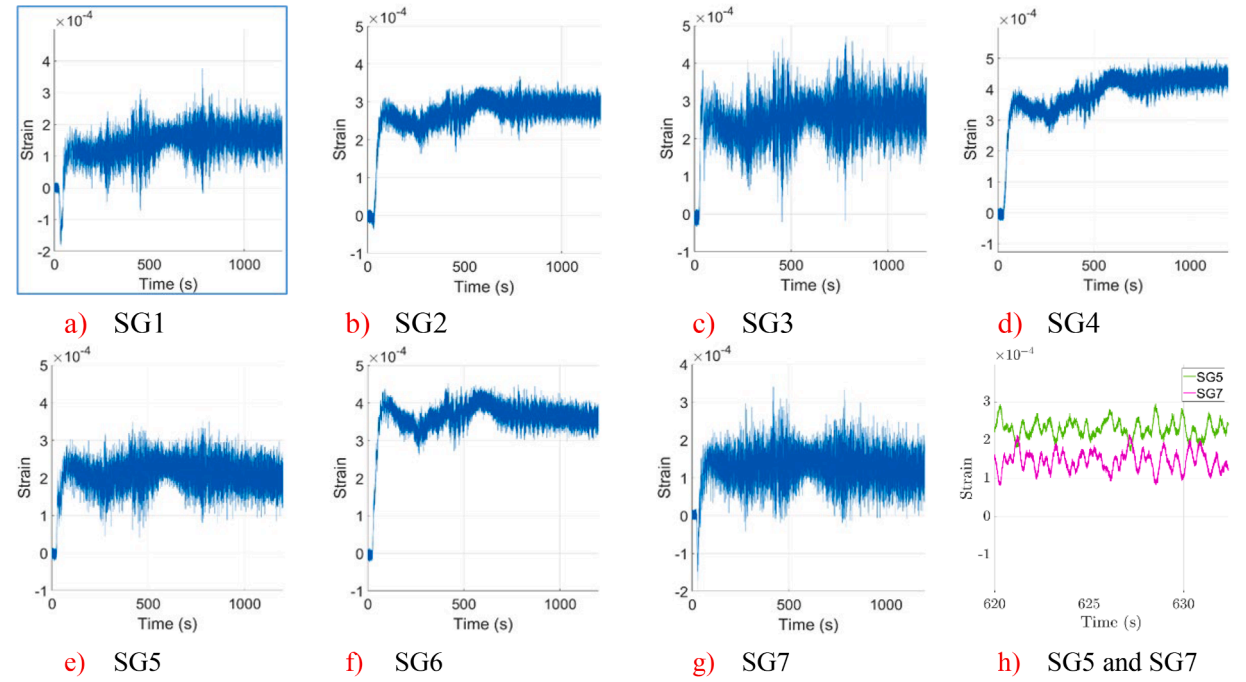

Fig. 15. showing the time histories of the strain gauges attached to the pipe as the flow inside the pipe transitioned from single phase to multi-phase (SP4-MP4). The stretching of the pipe, which results from the additional weight of water in the pipe leads to the stretching of the pipe.

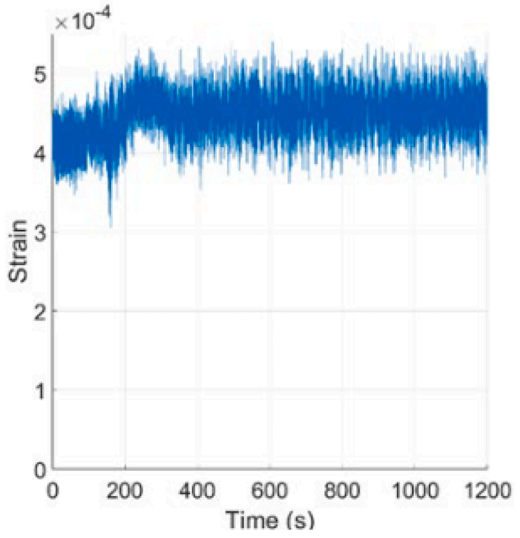

Fig. 16. showing the time history of the strain gauge SG4 as the flow inside the pipe transitioned from multi-phase tespt point MP4-MP2.

was maintained at $Q_g = 18.25\ m^3/hr$ and the liquid flow rate, Q_l, was increased in steps from 0 m^3/hr to 14.5 m^3/hr. The mean strains experienced by most of the strain gauges on the riser increased as the liquid flow rate increased from 5.5 to 14.5 m^3/hr. It is believed that the variation in the mean strains experienced by the riser occurs because of the increased amount of water in the pipe, which therefore affects its weight. This in turn determined a different minimum energy profile for the pipe as the mass contained within it changed and thus applied additional strain to the pipe.

Analysis of Fig. 17b shows that increasing the liquid flow rate increased the unsteadiness of the strains experienced by the flexible riser at both the bottom and top of the riser. As a result of the pipes movement, which was predominantly in-plane, the strain experienced by the strain gauges mounted in-plane (SG1, SG3, SG5 and SG7) were larger than those measuring the out of plane strain. The peak strain experienced by the pipe occurred on the underside of the pipe at the top of the riser, for test point MP3. This

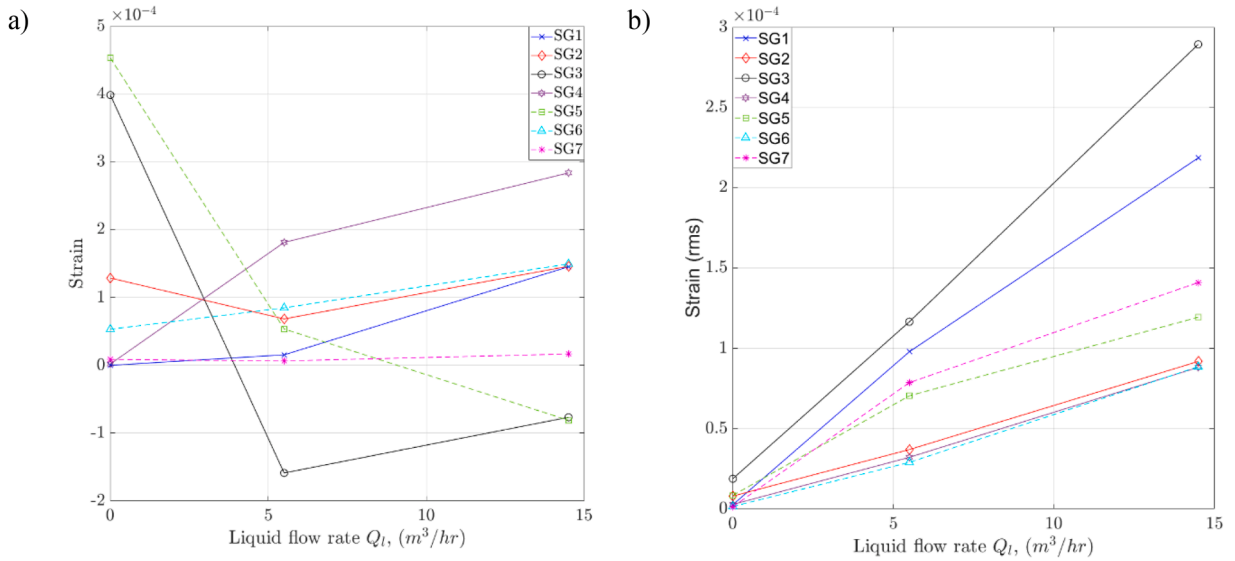

Fig. 17. Showing a) the mean strain and b) the RMS of the fluctuations of the strain gauge data about the mean are presented when the gas flow rate is kept constant, and the liquid flow rate varied.

corresponds with the large pipe displacements described earlier by the accelerometer data, and the whip-like motion of the pipe (see Fig. 19). The very small variation in the unsteadiness of the coupled, out-of-plane, strain gauges (SG2-SG4) indicates that at the bottom of the riser the pipe did not deform out-of-plane. Unfortunately, due to the failure of SG8 it is not possible to determine if there is a significant amount of deformation of the riser at the top. The unsteadiness of the coupled, in-plane, strain gauges (SG1-SG3, SG5-SG7) indicates that the pipe deforms in-plane due to its motion. This observation confirms the results from the analysis of the accelerometers.

For both data sets presented, this corresponds with an observable change in the motion of the pipe when $Q_l = 14.5\ m^3/hr$ and $Q_g = 18.25\ m^3/hr$ (MP3). This presents an interesting development whereby at higher flow rates (for either liquid or gas) the movement of the pipe became greater towards the central region of the pipe. For all other test points, the lower section of the pipe moved in a consistent fashion, in-plane, oscillating up and down smoothly as a result of the slug flow inside of the pipe. A representation of the motion of the pipe for low to moderate flow rates is presented for visualization purposes in Fig. 18b and c. This was created by compiling the pipe profiles extracted from the sequential images shown in Fig. 18a.

For MP3, the motion could occasionally become jerky and whip-like, with increased amplitude observed towards the central region of the riser section. At the bottom of the riser, the slug flow generated a large vertical oscillation, however, after an unknown number of slugs, the flow appears to generate a much larger pipe displacement. The larger vertical displacement generates some slack in the higher up section on the riser, which therefore sags backward. Upon the generation of this slack, the lower section of the riser returns to its original location, generating a violent tugging motion on the riser. This motion is notionally similar to that of a whip. This result is in agreement with the results of the smaller laboratory scale experiment investigated by Cavalcante et al. who uncovered that a whipping motion increased as the gas superficial velocity increase for a fixed liquid superficial velocity (Cavalcante et al., 2007). After the in-plane whipping motion occurs, the pipe starts to move out-of-plane. This process can been see in the sequential images and the sketches shown as a sketch in Fig. 19. It is believed that the rigid fixed ends of the flexible riser prevented the whiplash from propagating further. To dissipate the energy within the pipe, the pipe moved out-of-plane such that the movement had generally dissipated by the time the pipe experienced its next whipping motion. Increased flow rates beyond those of MP3 were predicted to show slug flow, but these tests were abandoned due to safety concerns as the amplitude of the waves and whipping effect increased to such an extent that the first such test point had to be stopped during testing.

Examination of Fig. 19b reveals a point at which all profiles overlap. This node was present in all multiphase flow test points but was most visible in MP3. This observation was also revealed in the accelerometer data, whereby the maximum peak to peak radial displacement experienced by AC2 was always larger than that of AC1 even though both measured the in-plane response. From Fig. 6 the position of AC1 is closer to the node position identified in Fig. 19b and so experiences lower displacement values. AC2 was positioned between the node and the fixed point at the base of the riser section.

The mean strain and the RMS of the fluctuations of the strain experienced by the flexible riser when the liquid flow rate was kept constant at $Q_l = 14.5\ m^3/hr$ and the gas flow rate varied from $Q_g = 5.5\ m^3/hr$ to $18.25\ m^3/hr$ are shown in Fig. 20. In agreement with Fig. 17a, maintaining the liquid flow rate while increasing the gas flow rate appeared to slightly reduce the mean strain experienced by each strain gauge (as can be seen in Fig. 20a). This reinforces the proposal that the decrease in the mean strains experienced by the riser occurs because of the proportionally lower mass of liquid in the pipe, producing the inverse of the result described previously.

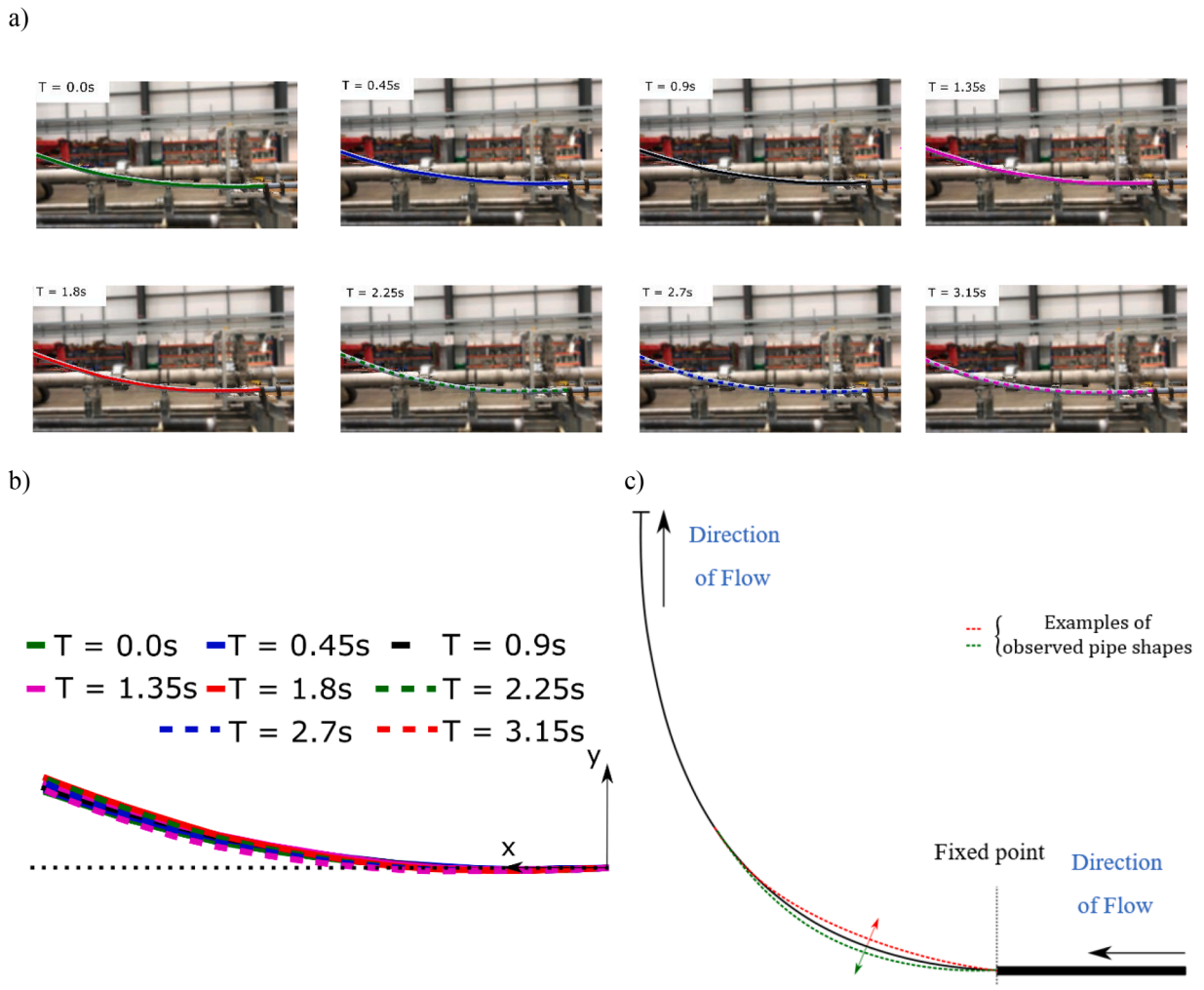

Fig. 18. (a) Sequential pictures of the pipe showing the shape it takes at low to moderate flow rates. (b) Overlays of the pipe shapes. (c) Sketch indicating the motion of the pipe motion at low to moderate flow rates.

5. Conclusions

An investigation into the effect nitrogen/water slug flow has on the structure of a flexible riser has been performed using surface mounted strain gauges, accelerometers, and high-speed cameras.

The results show that under single-phase gas flow conditions, the flexible J-riser did not move significantly, but when multiphase slug flow travelled through the system, significant pipe movements were observed. The experimental data show that the flexible riser moved predominantly in the plane of the pipe, but some out-of-plane motion was observed at higher flow rates.

For low rates, pipe movement was more evenly distributed between the lower to the central region. This motion was typified by an in-plane continuous smooth oscillation of the pipe as the slug flow passed through it. A node was observed at a consistent location through both camera and accelerometer data. At the increased rates, the smooth motion was sporadically interrupted by jerky and whip-like movement with higher amplitude of the J-riser. This caused a tugging motion on the upper rigid piping at the clear viewing section and beyond, which resulted in significant movement being observed in that section.

Investigating the flow regime map and filtering the resulting test points through PETEX GAP software and then through CFD simulations yielded a test matrix which produced the desired flow regime in all cases tested. Caution should be used when applying CFD modelling of a rigid model to a flexible system. For the exclusive purpose of determining the flow regime in a geometry that does not perfectly fit standard flow regime maps, this study has demonstrated that CFD can be successfully applied. However, to determine slug features correctly, application of a fully two-way coupled Fluid/Structure model should be applied, but this is beyond the scope of this experimental study. It would provide a useful future work to apply such a model and validate against the slug features, strains and deformations reported here. Slug length varied from 0.16 *m* to greater than 3.8 *m*. Increasing gas flow rate while holding liquid flow rate constant saw a general increase in slug length for either gas or liquid slugs. Though for the highest gas flow rate, there was a departure from this trend, and significant increase in the standard deviation, demonstrating a larger variation in this parameter. It is

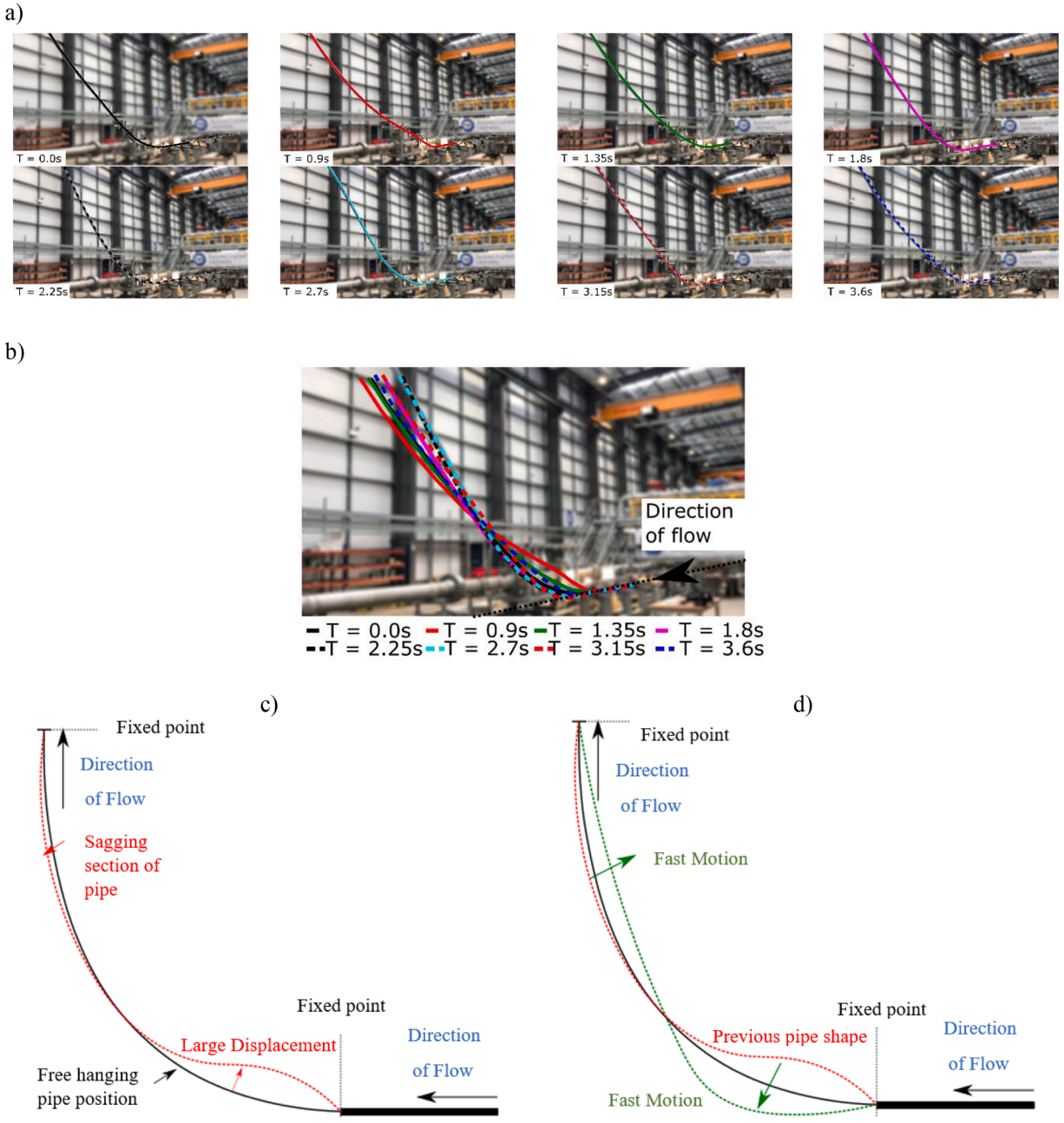

Fig. 19. (a) Sequential pictures of the pipe showing the whipping motion of the pipe. (b) Overlays of the pipe shapes (c) and (d) Sketch indicating the whipping motion of the pipe.

proposed that this derives from structure-fluid interaction due to the increased movement and sporadic whipping motion of the flexible section.

For increased liquid flow rate (at constant gas flow rate), the average value of the strain was seen to increase. Likewise, an increase in the flow rate of gas (at constant liquid flow rate) resulted in a decrease in the mean strain. It is probable that the cause of this is due to the flexible pipe adopting a distinct minimum energy configuration for each increase in liquid flow rate due to increased mass in the pipe. An increase in flow rates of either liquid or gas (under a constant flow rate condition for the other phase) saw the radial displacement and strain caused by the movement of the pipe to increase. This is reflected in the RMS values of the fluctuations for strain in all cases.

The passage of slugs from the riser to the upper viewing section caused either an obfuscation of the slug behind smaller bubbles or a true churn flow. This ambiguity suggests the topic of future work and extensive examination of the high-speed camera images to see if a

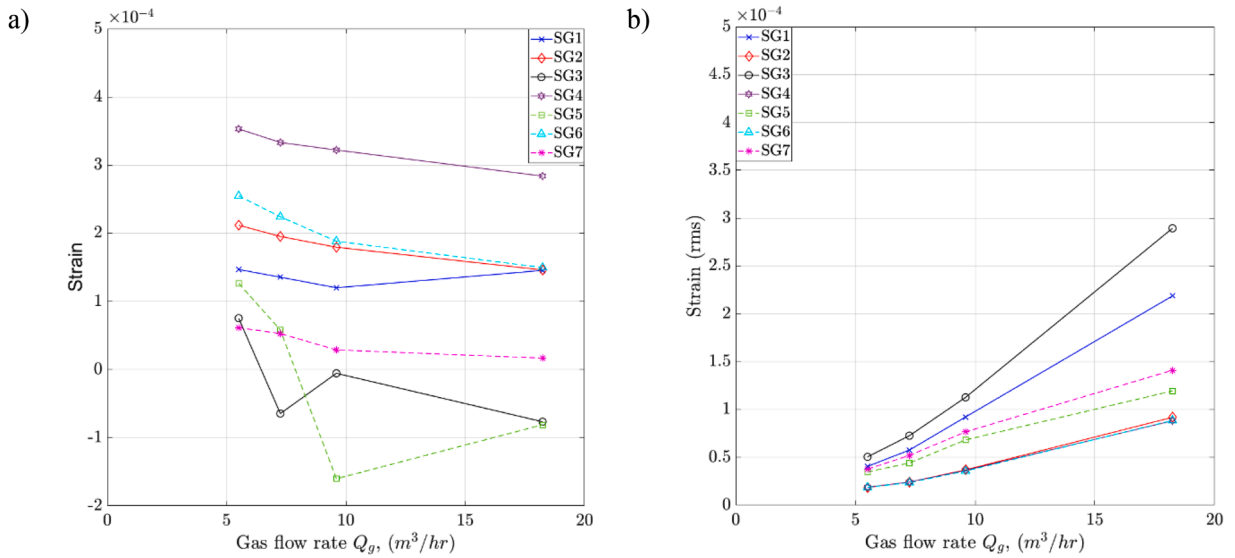

Fig. 20. Showing a) the mean strain and b) the RMS of the fluctuations of the strain gauge data about the mean are presented when the liquid flow rate is kept constant, and the gas flow rate varied.

definite conclusion can be reached. Though half of the test points were predicted in the vertical flow regime map as annular dispersed flow, the flow experienced alternated from bubbly to churn with the passage of slugs for all test points. Of additional interest, the transition of a slug through the vertical viewing section repeatedly induced a reversed flow phenomenon in the liquid phase.

The results of this work offer new insights into fluid-structure interactions in large scale engineering applications. They contribute to minimising uncertainty in the identification of the likelihood of fatigue failure and the associated safety and environmental risks, and hence to delivering improved system design and control.

CRediT authorship contribution statement

D.J. Pickles: Data curation, Formal analysis, Investigation, Methodology, Software, Validation, Visualization, Writing – original draft, Writing – review & editing. **G. Hunt:** Formal analysis, Investigation, Software, Validation, Visualization, Writing – original draft, Writing – review & editing. **A.J. Elliott:** Formal analysis, Methodology, Software, Validation. **A. Cammarano:** Conceptualization, Investigation, Project administration, Supervision, Visualization, Writing – review & editing. **G. Falcone:** Conceptualization, Funding acquisition, Investigation, Project administration, Supervision, Visualization, Writing – review & editing.

Declaration of competing interest

The authors declare that they have no known competing financial interests or personal relationships that could have appeared to influence the work reported in this paper.

Data availability

Data will be made available on request.

Acknowledgments

The authors are grateful for the funding support from the Engineering and Physical Sciences Research Council (EPSRC) of UK Research and Innovation through the “MUltiphase Flow-induced Fluid-flexible structure InteractioN in Subsea applications (MUFFINS)” project grant EP/P033148/1. The authors would like to thank the assistance provided by the EPSRC RELIANT, Risk EvaLuatIon fAst iNtelligent Tool for COVID19 (No. EP/V036777/1). Finally, the authors would also like to acknowledge the TÜV SÜD National Engineering Laboratory for their assistance with implementing the bespoke loop design.

References

Abdulkadir, M., Mbalisigwe, U.P., Zhao, D., Hernandez-Perez, V., Azzopardi, B.J., Tahir, S., 2019. Characteristics of churn and annular flows in a large diameter vertical riser. Int. J. Multiphase Flow 113, 250–263. https://doi.org/10.1016/J.IJMULTIPHASEFLOW.2019.01.013.

Al-Hashimy, Z.I., Al-Kayiem, H.H., Kadhim, Z.K., Mohmmed, & A.O., 2015. Numerical simulation and pressure drop prediction of slug flow in oil/gas pipelines computational methods in multiphase flow VIII 57. WIT Trans. Eng. Sci. 89 https://doi.org/10.2495/MPF150051.
Al-Hashimy, Z.I., Al-Kayiem, H.H., Time, R.W., Kadhim, Z.K., 2016. Numerical characterisation of slug flow in horizontal air/water pipe flow. Internat. J. Comput. Meth. Experiment. Measure. 4, 114–130. https://doi.org/10.2495/CMEM-V4-N2-114-130.
Asiegbu, N.M., Hossain, M., Droubi, G.M., Islam, S.Z., 2023. Investigation of the effects of pipe diameter of internal multiphase flow on pipe elbow vibration and resonance. Proc. Inst. Mech. Eng. Part E J. Process Mech. Eng. 237, 1319–1330. https://doi.org/10.1177/09544089221115520/ASSET/IMAGES/LARGE/10.1177_09544089221115520-FIG8.JPEG.
Barnea, D., Shoham, O., Taitel, Y., Dukler, A.E., 1980. Flow pattern transition for gas-liquid flow in horizontal and inclined pipes comparison of experimental data with theory. Int. J. Multiph. Flow 6, 217–225.
Belfroid, S.P.C., Cargnelutti, M.F., Schiferli, W., Van Osch, M., 2011. Forces on bends and T-Joints due to multiphase flow. american society of mechanical engineers. Fluids Engin. Div. (Publication) FEDSM 3, 613–619. https://doi.org/10.1115/FEDSM-ICNMM2010-30756.
Brackbill, J.U., Kothe, D.B., Zemach, C., 1992. A continuum method for modeling surface tension. J. Comput. Phys. 100, 335–354. https://doi.org/10.1016/0021-9991(92)90240-Y.
Cavalcante, C.C.P., Bordalo, S.N., Morooka, C.K., Matt, C.G.C., Franciss, R., 2007. Experimental investigation on a laboratory-scale model of the fluid-pipe interaction on catenary risers for offshore petroleum production. portalabpg.org.brCCP Cavalcante, SN Bordalo, CK Morooka. CGC Matt, R. FrancissBrazilian J. Petrol. Gas 1, 78–87, 2008•portalabpg.org.br.
Chen, W., Ji, C., Srinil, N., Yan, Y., Zhang, Z., 2022. Effects of upstream wake on vortex-induced vibrations and wake patterns of side-by-side circular cylinders. Mar. struct. 84, 103223 https://doi.org/10.1016/J.MARSTRUC.2022.103223.
Chinenye-Kanu, N.M., Hossain, M., Droubi, M.G., Islam, S.Z., 2019. Numerical investigation of two-phase flow induced local fluctuations and interactions of flow properties through elbow. Lect. Notes Mech. Engin. 124–141. https://doi.org/10.1007/978-981-13-2273-0_11/FIGURES/16.
Duan, J.long, Chen, K., You, Y.xiang, Gao, S., 2017. Experimental and computational investigations on severe slugging in a catenary riser. China Ocean Engin. 31, 653–664. https://doi.org/10.1007/s13344-017-0075-5.
Dukler, A.E., Hubbard, M.G., 1971. A Model for gas-liquid slug flow in horizontal and near horizontal tubes. Trouton, F. T., Proc. Roy. Soc. Ser. A 10, 465.
Frank, T., 2005. The 11 The international topical meeting on nuclear reactor thermal-hydraulics (NURETH-11) Numerical Simulation Of Slug Flow Regime For An Air-Water Two-Phase Flow In Horizontal Pipes.
Garcia, C., Nemoto, R., Pereyra, E., Korelstein, L., Sarica, C., 2023. Hydrodynamic forces in a horizontal-horizontal elbow in a gas-liquid system hydrodynamic force flow-induced force flow-induced vibration multiphase flow flow pattern slug pseudo-slug flow density flow velocity flow frequency. Int. J. Multiphase Flow 159, 104321. https://doi.org/10.1016/j.ijmultiphaseflow.2022.104321.
Gourma, M., Verdin, P.G., 2020. Nature and magnitude of operating forces in a horizontal bend conveying gas-liquid slug flows. J. Pet. Sci. Eng. 190 https://doi.org/10.1016/J.PETROL.2020.107062.
Gourma, M., Verdin, P.G., 2016. Two-phase slug flows in helical pipes: slug frequency alterations and helicity fluctuations. Int. J. Multiphase Flow 86, 10–20. https://doi.org/10.1016/j.ijmultiphaseflow.2016.07.013.
Flow regime map for two-phase flow | excel calculations [WWW Document], 2011. URL http://excelcalculations.blogspot.com/2012/02/flow-regime-map.html (accessed 10.4.22).
Hara, F., 1973. A theory on the two-phase flow induced vibrations in piping systems.
Hara, F., Yamashita, T., 1978. Parallel two-phase-flow-induced vibrations in fuel pin model. J. Nucl. Sci. Technol. 15, 346–354. https://doi.org/10.1080/18811248.1978.9735520.
Heaney, C.E., Wolffs, Z., Tómasson, J.A., Kahouadji, L., Salinas, P., Nicolle, A., Navon, I.M., Matar, O.K., Srinil, N., Pain, C.C., 2022. An AI-based non-intrusive reduced-order model for extended domains applied to multiphase flow in pipes. Phys. Fluids 34, 55111. https://doi.org/10.1063/5.0088070/2847368.
Hernandez-Perez, V., Abdulkadir, M., Azzopardi, B.J., 2011. Grid generation issues in the CFD modelling of two-phase flow in a pipe. J. Comput. Multi. Flows 3, 13–26. https://doi.org/10.1260/1757-482X.3.1.13.
Hirt, C.W., Nichols, B.D., 1981. Volume of fluid (VOF) method for the dynamics of free boundaries. J. Comput. Phys. 39, 201–225. https://doi.org/10.1016/0021-9991(81)90145-5.
Jagan, V., Satheesh, A., 2016. Experimental studies on two phase flow patterns of air–water mixture in a pipe with different orientations. Flow Meas. Instrum. 52, 170–179. https://doi.org/10.1016/J.FLOWMEASINST.2016.10.006.
Khan, U., Pao, W., Sallih, N., 2022. A review: factors affecting internal two-phase flow-induced vibrations. Applied Sciences (Switzerland) 12. https://doi.org/10.3390/APP12178406.
Liu, Y., Miwa, S., Hibiki, T., Ishii, M., Morita, H., Kondoh, Y., Tanimoto, K., 2012. Experimental study of internal two-phase flow induced fluctuating force on a 90° elbow. Chem. Eng. Sci. 76, 173–187. https://doi.org/10.1016/J.CES.2012.04.021.
Mahrenholtz, Oskar., Markiewicz, Maciej., 1999. Nonlinear water wave interaction. WIT Press, Southampton.
Malekzadeh, R., Henkes, R.A.W.M., Mudde, R.F., 2012. Severe slugging in a long pipeline-riser system: experiments and predictions. Int. J. Multiphase Flow 46, 9–21. https://doi.org/10.1016/j.ijmultiphaseflow.2012.06.004.
Matamoros, L.M.C., Loureiro, J.B.R., Silva Freire, A.P., 2014. Length–area–volume of long bubbles in horizontal slug flow. Int. J. Multiphase Flow 65, 24–30. https://doi.org/10.1016/J.IJMULTIPHASEFLOW.2014.05.007.
Mayor, T.S., Pinto, A.M.F.R., Campos, J.B.L.M., 2007. An image analysis technique for the study of gas-liquid slug flow along vertical pipes - associated uncertainty. Flow Meas. Instrum. 18, 139–147. https://doi.org/10.1016/j.flowmeasinst.2007.05.004.
Menter, F.R., 1994. Two-equation eddy-viscosity turbulence models for engineering applications. AIAA J. 32, 1598–1605. https://doi.org/10.2514/3.12149.
Miwa, S., Hibiki, T., Mori, M., 2016. Analysis of flow-induced vibration due to stratified wavy two-phase flow. J. Fluids Engin., Transact. ASME 138. https://doi.org/10.1115/1.4033371/444559.
Miwa, S., Mori, M., Hibiki, T., 2015. Two-phase flow induced vibration in piping systems. Prog. Nucl. Energy 78, 270–284. https://doi.org/10.1016/J.PNUCENE.2014.10.003.
Mohmmed, A.O., Al-Kayiem, H.H., Osman, A.B., Sabir, O., 2020. One-way coupled fluid–structure interaction of gas–liquid slug flow in a horizontal pipe: experiments and simulations. J. Fluids Struct. 97 https://doi.org/10.1016/J.JFLUIDSTRUCTS.2020.103083.
Monette, C., Pettigrew, M.J., 2004. Fluidelastic instability of flexible tubes subjected to two-phase internal flow. J. Fluids Struct. 19, 943–956. https://doi.org/10.1016/J.JFLUIDSTRUCTS.2004.06.003.
Ortiz-Vidal, L.E., Mureithi, N.W., Rodriguez, O.M.H., 2017. Vibration response of a pipe subjected to two-phase flow: analytical formulations and experiments. Nucl. Eng. Des. 313, 214–224. https://doi.org/10.1016/J.NUCENGDES.2016.12.020.
Padrino, J.C., Srinil, N., Kurushina, V., Swailes, D., 2023. International Journal of Multiphase Flow Prediction of unsteady slug flow in a long curved inclined riser with a slug tracking model. Int. J. Multiphase Flow 162, 104410. https://doi.org/10.1016/j.ijmultiphaseflow.2023.104410.
Patel, M.H., Seyed, F.B., 1989. Internal flow-induced behaviour of flexible risers. Eng. Struct. 11, 266–280. https://doi.org/10.1016/0141-0296(89)90046-1.
Pettigrew, M.J., Taylor, C.E., Fisher, N.J., Yetisir, M., Smith, B.A.W., 1998. Flow-induced vibration: recent findings and open questions. Nucl. Eng. Des. 185, 249–276. https://doi.org/10.1016/S0029-5493(98)00238-6.
Ratkovich, N., Majumder, S.K., Bentzen, T.R., 2013. Empirical correlations and CFD simulations of vertical two-phase gas–liquid (Newtonian and non-Newtonian) slug flow compared against experimental data of void fraction. Chem. Eng. Res. Des. 91, 988–998. https://doi.org/10.1016/J.CHERD.2012.11.002.
Riverin, J.L., de Langre, E., Pettigrew, M.J., 2006. Fluctuating forces caused by internal two-phase flow on bends and tees. J. Sound Vib. 298, 1088–1098. https://doi.org/10.1016/j.jsv.2006.06.039.
Riverin, J.L., Pettigrew, M.J., 2007. Vibration excitation forces due to two-phase flow in piping elements. undefined 129, 7–13. https://doi.org/10.1115/1.2388994.
Sadeghi, H., Diosady, L., Blais, B., 2022. A computational fluid dynamics study on rimming flow in a rotating cylinder. Phys. Fluids 34, 063304. https://doi.org/10.1063/5.0093351.

Schlegel, J.P., Miwa, S., Chen, S., Hibiki, T., Ishii, M., 2012. Experimental study of two-phase flow structure in large diameter pipes. Exp. Therm Fluid Sci. 41, 12–22. https://doi.org/10.1016/J.EXPTHERMFLUSCI.2012.01.034.

Tay, B.L., Thorpe, R.B., 2004. Effects of liquid physical properties on the forces acting on a pipe bend in gas–liquid slug flow. Chem. Eng. Res. Des. 82, 344–356. https://doi.org/10.1205/026387604322870453.

Wang, L., Yang, Y., Li, Y., Wang, Y., 2018a. Dynamic behaviours of horizontal gas-liquid pipes subjected to hydrodynamic slug flow: modelling and experiments. Int. J. Press. Vessels Pip. 161, 50–57. https://doi.org/10.1016/J.IJPVP.2018.02.005.

Wang, L., Yang, Y., Liu, C., Li, Y., Hu, Q., 2018b. Numerical investigation of dynamic response of a pipeline-riser system caused by severe slugging flow. Int. J. Press. Vessels Pip. 159, 15–27. https://doi.org/10.1016/J.IJPVP.2017.11.002.

Widyatama, A., Dinaryanto, O., 2016. The application of digital image processing to study slug flow characteristics in a horizontal pipe. Internat. J. Engin. Techn. 8, 2654–2663. https://doi.org/10.21817/ijet/2016/v8i6/160806222.

UK National Measurement System - GOV.UK [WWW Document], 2022. URL https://www.gov.uk/government/publications/national-measurement-system/uk-national-measurement-system (accessed 10.6.23).

Xu, W., Zhang, S., Ma, Y., Liu, B., 2020. Fluid forces acting on three and four long side-by-side flexible cylinders undergoing flow-induced vibration(FIV). https://doi.org/10.1016/j.marstruc.2020.102877.

Yang, Y., Li, J., Wang, S., Wen, C., 2018. Gas-liquid two-phase flow behavior in terrain-inclined pipelines for gathering transport system of wet natural gas. Int. J. Press. Vessels Pip. 162, 52–58. https://doi.org/10.1016/J.IJPVP.2018.03.005.

Yih, T., Griffith, P., 1968. Unsteady momentum fluxes in two-phase flow and the vibration of nuclear reactor components.

Zhang, N., Li, S., Sun, B., Huang, C., Huang, K., Zeng, Y., Liu, C., 2023. Flexible riser tensile armor modelling method and application to fatigue analysis. J. Marine Sci. Engin. 2023 11, 1500. https://doi.org/10.3390/JMSE11081500. Page 1500 11.

Zhu, H., Gao, Y., Zhao, H., 2019. Experimental investigation of slug flow-induced vibration of a flexible riser. Ocean Eng. 189, 106370 https://doi.org/10.1016/J.OCEANENG.2019.106370.

Zhu, H., Gao, Y., Zhao, H., 2018. Experimental investigation on the flow-induced vibration of a free-hanging flexible riser by internal unstable hydrodynamic slug flow. Ocean Eng. 164, 488–507. https://doi.org/10.1016/J.OCEANENG.2018.06.071.

Zhu, H., Hu, J., Gao, Y., 2021a. Severe slug flow-induced nonlinear dynamic behavior of a flexible catenary riser. Phys. Fluids 33, 71705. https://doi.org/10.1063/5.0054160/990065.

Zhu, H., Hu, J., Gao, Y., Zhao, H., Xu, W., 2021b. Spatial–temporal mode transition in vortex-induced vibration of catenary flexible riser. J. Fluids Struct. 102, 103234 https://doi.org/10.1016/J.JFLUIDSTRUCTS.2021.103234.